AD-A032 492 PURDUE UNIV LAFAYETTE IND PROJECT SQUID HEADQUARTERS F/G 20/6
APPICABILITY OF LASER RAMAN SCATTERING DIAGNOSTIC TECHNIQUES TO--ETC(U)
OCT 76 A C ECKBRETH
UNCLASSIFIED SQUID-TR-UTRC-4-PU N00014-75-C-1143
NL

1 OF 1
AD A032492

(12)
NW

PROJECT SQUID
TECHNICAL REPORT UTRC-4-PU

APPLICABILITY OF LASER RAMAN SCATTERING DIAGNOSTIC TECHNIQUES TO PRACTICAL COMBUSTION SYSTEMS

BY

ALAN C. ECKBRETH
UNITED TECHNOLOGIES RESEARCH CENTER
EAST HARTFORD, CONNECTICUT

PROJECT SQUID HEADQUARTERS
CHAFFEE HALL
PURDUE UNIVERISTY
WEST LAFAYETTE, INDIANA 47907

OCTOBER 1976

Project SQUID is a cooperative program of basic research relating to Jet Propulsion. It is sponsored by the Office of Naval Research and is administered by Purdue University through Contract N00014-75-C-1143, NR-098-038.

R76-952396-2

PROJECT SQUID

TECHNICAL REPORT UTRC-4-PU

A COOPERATIVE PROGRAM OF FUNDAMENTAL RESEARCH
AS RELATED TO JET PROPULSION
OFFICE OF NAVAL RESEARCH, DEPARTMENT OF THE NAVY

CONTRACT (15) N00014-75-C1143 NR-098-038

(6) APPLICABILITY OF LASER RAMAN SCATTERING DIAGNOSTIC TECHNIQUES TO PRACTICAL COMBUSTION SYSTEMS.

(9) Technical rept. 28 Jan–31 Aug 76

(10) by ALAN C. ECKBRETH
UNITED TECHNOLOGIES RESEARCH CENTER
EAST HARTFORD, CONNECTICUT 06108

(11) OCTOBER 1976

(12) 97 p.

(14) SQUID-TR-UTRC-4-PU

PROJECT SQUID HEADQUARTERS
CHAFFEE HALL
PURDUE UNIVERSITY
WEST LAFAYETTE, INDIANA

1473

403617 LB

TABLE OF CONTENTS

TABLE OF CONTENTS (CONT'D)

LIST OF ILLUSTRATIONS

LIST OF ILLUSTRATIONS(CONT'D)

LIST OF TABLES

SUMMARY

Laser Raman scattering techniques for combustion diagnosis have undergone considerable development in the past several years and are now being employed in a number of fundamental flame investigations. However, from an instrumentation viewpoint, practical combustion environments can differ greatly from the flames typically employed in fundamental studies. In particular, pulsed laser Raman thermometry experiments have shown laser modulated particulate (soot) incandescence to be an especially severe problem. Particles in the measurement volume, which, at flame temperatures, are already incandescent and contribute significantly to the total luminous emission, absorb the incident Raman inducing laser radiation, heat to temperatures far above ambient, and emit greatly increased amounts of gray/blackbody radiation which can exceed the sought-for Raman signal levels by several orders of magnitude. Under Project SQUID sponsorship, a detailed study of this phenomenon has been conducted, the results of which are reported herein. Laser irradiated particulate temperatures were determined in a laminar propane diffusion flame as a function of focal flux level and found to agree fairly well with a simple analytical model. In addition to incandescence, laser induced C_2 Swan emissions were also found to be present. The laser induced particulate incandescent noise was found to saturate with increasing laser energy and to decrease in magnitude with shorter focussing lens focal length. Extrapolated improvements in signal to noise ratio with increasing flux levels from $2(10^5)$ to 10^9 W/cm^2 were on the order of a few hundred. The effect of signal averaging Raman data obtained from harsh (luminous, sooty) fluctuating media was analyzed. Ensemble

averaging pulsed Raman data leads to quantities dependent not only on average temperature but also on the magnitude and correlations of fluctuations in density and temperature, which can affect measurement accuracy. Temperature measurements were made on a clean flame and a temperature measurement demonstration was performed on a soot seeded laboratory burner using a noise sampling and subtraction approach.

INTRODUCTION

With the development of high power, visible laser sources, Raman scattering diagnostic techniques have received considerable attention for combustion diagnostics in the past several years (Ref. 1). Laser Raman approaches have been advanced to the point where they are now being routinely employed for fundamental flame investigations (Refs. 2, 3). However, widespread application of laser Raman techniques to practical combustion devices such as gas turbines, hydrocarbon combustors, furnaces, etc., is yet to be achieved. From an instrumentation standpoint, flames of practical interest differ markedly from the flames typically examined in fundamental laboratory studies. Environments of practical interest contain flames which are generally turbulent, highly luminous and particulate laden. These conditions lead to a variety of problems, all of which can adversely affect the successful application of a particular laser Raman technique. These problems arise due to the extremely low cross sections for spontaneous Raman scattering, typically in the range of $1\text{-}10(10^{-31})$ cm^2/sr. As a result, spontaneous Raman signals are extremely weak and are easily masked by extraneous light emissions from a variety of sources such as: Background Luminosity The turbulent diffusion flames utilized in practical devices are extremely luminous due to a combination of chemiluminescent and particulate radiations. Using the instrument and combustor described in Refs. 4, 5 the radiative power density with propane fuel at 5200Å was on the order of 100 (10^{-9}) $Watts/cm^3$ Å sr depending on stoichiometry. Such power levels rule out the use of cw laser sources for Raman work in these environments and can lead to low S/N even for powerful pulsed laser sources. Laser Induced Particulate Effects In situations where the background luminosity is tolerable or adequately

suppressed by filtering or geometric design, the pulsed laser-particulate interaction can lead to a variety of noise effects such as fluorescence, incandescence (due to laser absorption and heating), and molecular emission which mask detection of the Raman data. In the secondary zone of the aforementioned combustor burning methane, laser induced particulate incandescence was found to be especially severe (Ref. 5). There the (Raman signal)/(laser induced particulate incandescence noise) ratio for a 25 kW peak power dye laser pulse was as low as 0.05. In the laminar propane diffusion flames studied herein, S/N ratios below 10^{-4} have been observed for 400 kW laser power levels as will be discussed subsequently. Further study reported herein has revealed that laser induced Swan emission (from vaporizing C_2) can be present in addition to incandescence. Severe laser induced hydrocarbon fluorescence has been encountered by Leonard (Ref. 6) in Raman experiments on a T53-L13A gas turbine engine exhaust. Turbulence can also be a source of problems. For the small combustor (12 cm dia) studied, little laser beam steering or defocussing was measured, but such effects could be problematical in larger devices. Since signal averaging is required in most situations, turbulent fluctuations can lead to averaging errors when band intensities need be averaged separately (Ref. 3).

Although the research under the subject contract has concentrated on the laser modulated particulate incandescence problem, solutions to this problem are applicable to those arising from background luminosity as well. In addition the effects of turbulent fluctuations on signal averaging are also treated, so that in a sense, all of the three major problem areas for spontaneous Raman scattering described above are addressed herein. The next section of this report briefly reviews the laser modulated

particulate incandenscence problem and presents an analysis of laser irradiated particle heating. More details on laser particulate interaction physics are presented in Ref. 5. Several potential solutions to this problem are described, two of which have been investigated under the contract. A third approach, investigated under corporate sponsorship (Ref. 7) is briefly described for completeness. Experiments on laser irradiated particle "noise" scaling are then described including discussions of appropriate particle seeding techniques. The problem of signal averaging pulsed Raman data from a turbulent medium is then addressed. Temperature measurements in a "noisy" flame are then presented employing one of the previously discussed techniques. The report ends with a series of conclusions and recommendations based upon the experimental and analytical investigations conducted. Appendix I includes a brief tutorial review of Raman scattering together with a discussion of the theoretical basis underlying its use for thermometry. Appendix II summarizes the computer code used to calculate Raman ratios as a function of temperature.

LASER MODULATED PARTICULATE INCANDESCENCE

Review of Laser Raman Thermometric Technique

Before proceeding to discuss the laser modulated particulate incandescence problem, the laser Raman thermometry approach employed in these studies will be briefly reviewed. For the reader unfamiliar with Raman scattering, a brief review is presented in Appendix I together with a discussion explaining its use for thermometry. The approach followed here is described in detail in Ref. 4 and depicted schematically in Fig. 1. The output from a dye laser (tuned to 5877Å) is introduced into the medium under study coaxially to the main light collecting optics by the series of mirrors, M. The spectrometer is arranged to detect vibrational Raman scattering from N_2, since N_2 is the dominant constituent in an airfed combustor. Scattering at right angles to the laser beam is also possible using a different optical routing not shown. The small lens, L, focuses the dye laser beam down in the region from which scattering is to be observed. Baffles and light tubes are employed to prevent the detection of any spurious scattering from within the spectrometer. Scattered light is collected at the focal length of the forward lens (10 cm diam, f/2.9), the collimator, which is translatable so that different sample volumes can be probed. The collimated output is focused down by a similar lens and recollimated to produce a 2.5 cm diam beam after the recollimator. The aperture, S, and obscuration disk, O, determine the spatial resolution (for backscattering) in the sample volume as described in Ref. 4. Beyond the recollimator, the scattered light passes through a trichroic, which passes the N_2 Stokes (6810Å) and anti-Stokes (5169Å) components and attenuates

by 10^{+4} light centered about the dye laser wavelength, e.g., Rayleigh, Mie scattering. Spectral separation of the signals is achieved by the dichroic, D. The Stokes signal then passes through 12 mm of Schott RG 630 glass which has an attenuation, based upon bulk absorption, of 10^{-20} at the dye laser wavelength. Mounted directly in front of the 31000A photomultiplier tube is a narrowband, 10Å or 50Å wide, interference filter. The anti-Stokes passes through several cut-off filters with an estimated 10^{8} rejection at the laser wavelength, through a 10Å wide narrowband filter to a 8575 photomultiplier. The PMT signals are amplified and sent to an oscilloscope (subsequent to some smoothing) for viewing or to an averager. Temperature is obtained from the ratio of the vibrational anti-Stokes to Stokes Raman intensities. Appendix II contains a description of the computer code used to determine the temperature dependence of the anti-Stokes to Stokes ratio for the experimental conditions pertaining.

The dye laser used for the combustor tests to be described subsequently is similar in design to that described in Ref. 8. After spectrally condensing and tuning with a low finesse multilayer dielectric etalon, the laser typically produced 25 millijoules in the Raman sample volume. The laser width (FWHM) was about 1 μsec. That laser has since been replaced with a Phase-R Co. Model DL-2100C which was employed in the experimental studies conducted under the contract.

Thermometry Experiments in Model Combustors

Laser Raman thermometry experiments were conducted in a hydrocarbon-fueled, axisymmetric model combustor employing coaxial injection of fuel and heated air shown in Fig. 2. The device was designed to display the essential features of many

practical combustors such as jet engines, industrial gas turbines, etc. More complete details in regard to the characteristics of this combustor are to be found in Ref. 9. In the tests to be described, the combustor was operated at 1 atm pressure with methane fuel and a mass flow rate of 0.140 kgm/sec. Measurements were attempted at window location 6.

The nature of the major problem encountered during these experiments is displayed in Fig. 3. The top trace displays the Stokes Raman signature obtained from ambient air at 300°K in the combustor prior to ignition. For reference, if after ignition, the combustor operated at 1500°K, the Stokes and anti-Stokes Raman signals would be approximately 14 percent and 21 percent, respectively of the 300°K Stokes signal. Note, however, that with the combustor operating, the signals actually obtained on the Raman channels are considerably larger than the 300°K Stokes signal and clearly do not arise from Raman scattering. The largest of these noise signals is about 20 times larger than the anticipated Raman signals. Although Mie scattering was initially suspected to be a possible cause of these spurious signals, it is the unlikely explanation for several reasons. Mie scattering would occur at the same wavelength as the incident laser light and, hence, reside outside the passbands of the spectrometer. Despite large Mie cross sections, the Raman spectrometer possesses more than enough rejection to suppress detecting even strong Mie scattering. Furthermore, the magnitude of the noise was sensitive to the spectrometer passband-width indicative of noise within the spectrometer passbands, not in the rejection zone. Lastly, Mie scattering is instantaneous and would exhibit the same temporal behavior as the laser and Raman signals. Examination of Fig. 3 reveals that the spurious signals exhibit a lag of approximately 0.5 μsec in peaking and about a 1-2 μsec tail.

The effect being seen is believed to be laser modulated particulate incandescence. Particulates (soot) in the measurement volume absorb the incident laser radiation, heat up and emit greatly increased amounts of broadband blackbody radiation. The plausibility of this mechanism is supported by comparing the amount of radiation a single particle can emit into the Raman passbands with the Raman scattering produced presented in Tables I and II respectively.

TABLE I

Particulate Blackbody Radiation Levels (Joules)

Signal Channel/Diameter (μ)	0.01	0.1	1	10
Anti-Stokes	3.13 (-21)	3.13 (-19)	3.13 (-17)	3.13 (-15)
Stokes	3.67 (-21)	3.67 (-19)	3.67 (-17)	3.67 (-15)

TABLE II

Collected Raman Energies (Joules)
25 mJ laser input energy

Signal Channel/Temperature	1500°K	2000°K
Anti-Stokes	1.63 (-16)	2.00 (-16)
Stokes	3.70 (-16)	2.75 (-16)

Laser Irradiated Particulate Heating

In Ref. 5 it is shown that except for low laser flux levels and the smallest particle sizes ($< 0.1\mu$), that heat conduction to the surrounding gaseous medium is insufficient to restrain the particle surface temperature from reaching the vaporization

temperature. Also, it can easily be shown that blackbody radiation is unimportant vis-a-vis the particle thermodynamics although it is a major problem to the Raman diagnostician. Consequently, only vaporization physics need be included in the particle heating analysis for the laser flux levels of interest here.

The analysis is similar to that employed by Chang , et al (Ref. 10). The continuity equation at the particle surface-gas interface is

$$\rho_s \frac{da}{dt} = \rho_v v_v \tag{1}$$

where a is the particle radius; ρ_s, particle density; ρ_v, the vapor density; and v_v, the vapor velocity. Equating the energy absorbed from the incident laser flux, q, to that consumed in vaporization yields

$$L \frac{dM}{dt} = \alpha\beta q \pi a^2 \tag{2}$$

where L is the latent heat of vaporization; M, the particle mass; α, the particle absorptivity, and β, a refractive index dependent term which accounts for reflection from the particles, assumed to be spherical for simplicity. Since

$$M = \frac{4}{3} \pi \rho_s a^3, \tag{3}$$

Eq. (2) may be rewritten

$$\rho_s \frac{da}{dt} = \frac{\alpha\beta q}{4L}. \tag{4}$$

The vapor velocity is assumed to be given by the Langmuir evaporation rate

$$v_v \approx \sqrt{\frac{kT_s}{2M_A}} \tag{5}$$

where M_A is the atomic mass of the vapor; k, Boltzmann's constant, and T_s, the particle surface temperature. It has been assumed here as in Ref. 11 that the vapor

at the surface is in thermal equilibrium with the surface temperature. For the velocities calculated from Eq. (5), it can be shown that the streaming energy term (Ref. 12) of the vapor can be neglected relative to the LHS of Eq. 2. The vapor pressure, p_v, dependence on surface temperature is obtained from the Clausius-Clapeyron equation

$$p_v = p_v^* \exp \frac{L(T_s - T_v^*)}{R_v T_s T_v^*} \tag{6}$$

where p_v^* is the vapor pressure at reference temperature T_v^*, and R_v, the gas constant. In the temperature range from 2000°K to 4000°K, C_3 is the major carbon vapor species, and together with the thermodynamic properties of carbon (Ref. 13) permits evaluation of Eq. (6). Combining the foregoing equations, the incident laser flux can be solved for explicitly as a function of particle surface temperature, viz.

$$q = \frac{4Lp_v^*}{\alpha\beta}\sqrt{\frac{M_A}{2kT_s}} \exp \frac{L(T_s - T_v^*)M_A}{kT_s T_v^*} \tag{7}$$

In Fig. 4, surface temperature is displayed as a function of laser flux using Eq. (7) for an atmospheric pressure combustor operating at 1500°K. As can be seen for laser fluxes in excess of 10^6 Watts/cm^2, superheating of the particles is predicted, i.e., the surface temperature exceeds the 1 atm vaporization temperature. Although superheating of the particulates is predicted, the surface temperature exhibits a relatively weak dependence on laser flux as shown.

Also shown in the figure are the surface temperatures predicted for conductive heat transfer to the gas balancing the incident laser radiation (Ref. 14)

$$T_s - T_o = \frac{\alpha\beta q a}{4k_a} \qquad (8)$$

where T_o is the initial particle surface temperature and k_a the thermal conductivity

Potential Solutions

The relevance of the foregoing analysis resides in the suggestion of solutions to the particulate noise problem and the evaluation it can provide of these possible solutions.

Optimal Laser Flux

The predicted variation of particle surface temperature with laser flux, Fig. 4, indicates that particulate emission will increase with increasing laser flux due to the increased particle surface temperatures which result. It might appear desirable then to operate at low laser flux levels. However, S/N considerations indicate just the opposite to be true. The Raman signal power, P_r, scales with incident laser power, P_i, in the well known manner (Ref. 1)

$$P_r = P_i n \frac{\partial\sigma}{\partial\Omega} \Omega \epsilon \ell \qquad (9)$$

where n is the number density of molecules in the initial scattering state; $\frac{\partial\sigma}{\partial\Omega}$, the Raman cross section; Ω, the collection solid angle; ℓ, the sampling extent; and ϵ, the collection efficiency. Alternately, the Raman power scales with flux, thusly,

$$S \sim qA \ell \qquad (10)$$

where A is the focal spot size of the incident laser beam.

The total amount of laser enhanced blackbody noise, N, emitted by a dispersion with a particle radius, a, distribution function n(a) is

$$N = \frac{2\pi(10^{-4})hc^2\Omega\Delta\lambda\epsilon A\ell}{\lambda^5\, 4\pi} \int_{a_1}^{a_2} \frac{a^2 n(a)}{e^{hc/kT_s\lambda} - 1}\, da \qquad (11)$$

where h is Planck's constant; c, the speed of light; and $\Delta\lambda$, the spectrometer bandwidth at wavelength λ. The noise is of course flux dependent through the temperature appearing in the exponential term of the Planck blackbody relation. The noise thus scales as

$$N \sim f(q)\, A\ell \qquad (12)$$

where f(q) represents the flux dependent temperature term in Eq. (11), namely the integral of $(e^{hc/kT\lambda} - 1)^{-1}$. The S/N

$$S/N \sim q/f(q) \qquad (13)$$

and is solely flux dependent. Because of the relatively weak variation of particle surface temperature with laser flux (Fig. 4), the S/N will increase with increasing laser flux. For example, the Fig. 3 data were obtained at a flux level of approximately $2(10^5)$ W/cm^2. From Eq. (13) the improvement in the S/N ratio, SNI, can be calculated for various levels of increased laser flux. The results are shown below in Table III for both the anti-Stokes and Stokes channels. The noise levels at the $2(10^5)$ W/cm^2 level were assigned a relative magnitude of unity.

TABLE III

SNI With Increasing Laser Flux

Flux(w/cm^2)	T_S(°K)	N_{AS}	SNI_{AS}	N_S	SNI_S
$2(10^5)$	3500	1.0	--	1.0	--
$2(10^6)$	4100	3.2	3.1	2.4	4.2
$2(10^7)$	4500	5.9	17.0	3.8	26.0
$2(10^8)$	5100	12.9	78.0	6.9	145.0
$2(10^9)$	5700	21.7	461.0	10.2	980.0

These SNI would lead to S/N in the range from 10-100 for the conditions previously studied at the highest laser flux levels assuming that the combustor gas breakdown threshold is not exceeded. For wavelengths in the visible and unclean air, breakdown is estimated to occur in the 10^9 to 10^{10} W/cm^2 flux range (Refs. 15, 16). Investigations of the scaling and magnitude of laser modulated particulate incandescence noise were a major focus of the experimental program conducted under the contract and will be described subsequently.

Noise Subtraction

Another possible solution to the particulate noise problem is to sample the noise in a spectral region adjacent to the Raman band simultaneously with the signal and to subtract the noise from the "Raman" signal. In the following analysis, the accuracy of this approach will be examined for shot noise limited detectors such as photomultipliers which are commonly employed in Raman work. It is assumed that both the signal and noise channels can be accurately calibrated relative to one another and that no error results from this consideration. The signals and typical relative

errors (due to photomultiplier shot noise) on both the "signal" and "noise" channels, assuming Poisson statistics (Ref. 17), can be written

$$S_s = \eta(n_s + n_n) \pm \sqrt{\eta(n_s + n_n)} \qquad (14)$$

$$S_n = \eta n_n \pm \sqrt{\eta n_n}$$

where η is the detector quantum efficiency; n_s, the number of signal photons, and n_n, the number of noise photons. Subtracting the "noise" channel from the "signal" channel leads to the true signal, ηn_s with a relative error of

$$RE = \frac{1 + \sqrt{1 + f}}{\sqrt{\eta n_s f}} \qquad (15)$$

where f is the average single shot S/N ratio, i.e., $\bar{n}_s/\bar{n}_n$.

Figure 5 displays the relative error or subtraction accuracy as a function of signal photon level for 20 percent quantum efficiency detectors and various S/N values. As can be seen, only for fairly large signal levels ($> 10^4$) can small relative errors be obtained even for S/N values of 10. For single pulse thermometry where two signals (e.g., anti-Stokes, Stokes) are ratioed to obtain temperature information, the relative error would approximately double. The actual error in temperature would be somewhat less generally due to the slope behavior of the ratio as a function of temperature. With a laser possessing both high flux levels (to increase f) and high pulse energy ($\gtrsim$1 Joule), a subtraction approach would offer improved temperature measurement accuracy. For example, with f $\approx$ 10 which would lead to single pulse temperature measurement accuracies of 15-20 percent, a subtraction

approach with a 10^4 photon signal level would lead to a measurement accuracy on the order of 5 percent. For single pulse thermometry and low f(< 1) subtraction approaches appear to be of marginal utility, however. A more detailed analysis of noise subtraction and the implications of signal averaging Raman data will be presented later in this report.

Raman Amplitude Modulation

From the previous discussion of laser irradiated particle heating (Ref. 5), it is clear that no significant phase behavior is exhibited by the particle surface temperature, which could be exploited in some manner to suppress the noise. Consequently phase behavior must be externally introduced into the experiment, either into the Raman signal or into the noise which can then be used in some manner to separate the signal from the noise. One such approach, investigated under corporate sponsorship (Ref. 7) and included here for completeness, is illustrated in Fig. 6. The technique involves rapid rotation of a polarized laser beam to amplitude modulate the Raman scattering. Most importantly, the technique avoids amplitude modulation of the incident laser beam which would lead to amplitude modulation of particulate incandescence and fluorescences and, thus, diminish the effectiveness of Raman a.m. detection.

The approach takes advantage of the polarization properties of vibrational Raman scattering exhibited by molecules with near vibration symmetry, e.g., N_2, namely, small depolarization ratios. In Fig. 6, the technique is illustrated for a right angle viewing geometry. It can also be implemented in other geometries, such as backscattering, by insertion of a polarization filter in the spectrometer.

The polarized laser pulse is passed through a Pockels cell driven to half wave voltage at high frequency. This rotates the polarization between 0^{o} and 90^{o} at a rate equal to twice the drive frequency. In Fig. 6, only the vertical component gives rise to significant Raman scattering leading to nearly complete amplitude modulation of the Raman scattering. For a dispersion of randomly oriented particles, laser induced incandescences and, possibly fluorescences as well, are not modulated since the absorption of radiation by the dispersion would not be expected to be polarization sensitive. Thus the noise would smoothly follow the laser pulse envelope exhibiting little or no phase behavior (Fig. 3). The drive frequency to the cell is chosen to be sufficiently greater than the characteristic high frequency components of the laser pulse spectrum. In the simplest embodiment of this approach, the modulated Raman signal riding on the smooth noise is separated from the latter by passage through a high frequency bandpass filter.

Under corporate sponsored programs, this approach has been experimentally evaluated. Amplitude modulated Raman scattering was produced and the laser induced particulate incandescence noise was found not to be amplitude modulated as initially hypothesized. However, upon bandpass filtering, very modest (< 10) improvements in S/N were obtained due to the photomultiplier shot noise on the laser induced particulate incandescence signal. Photomultiplier shot noise is essentially the variation in the photomultiplier output signal arising from the statistical nature of the photon detection process at the photocathode (Ref. 17). The shot noise is nearly spectrally white in character extending to the upper frequency response limit of the photomultiplier (Ref. 18). The improvement in S/N through filtering can be

crudely estimated using the following scheme. The initial S/N may be written as n_s/n_B where n_s and n_B are the total number of signal and background photons incident on the tube during the pulse time τ. Due to the 50% duty factor, the number of signal photoelectrons generated during a characteristic response time t_r of the photomultiplier is $\frac{1}{2}\eta n_s \frac{t_r}{\tau}$, where η is the tube quantum efficiency. The response time, t_r, is the width of the photoelectron output resulting from a light impulse and arises due to the photoelectron transit time spread through the dynode chain. It is related to the upper frequency response of the PMT, f_r, roughly as $f_r = \frac{1}{2}t_r$. Likewise the number of noise photoelectrons is $\eta n_B \frac{t_r}{\tau}$, and the shot noise $\sqrt{\eta n_B \frac{t_r}{\tau}}$. The amount of shot noise, assumed spectrally white, passing through the filter is then $\sqrt{\eta n_B \frac{t_r}{\tau}}\, \Delta f/f_r$ where Δf is the bandwidth of the filter. Hence the SNI (S/N improvement) through filtering is

$$\text{SNI} = (\tfrac{1}{2}\eta n_s \frac{t_r}{\tau})/(\sqrt{\eta n_B \frac{t_r}{\tau}}\, \frac{\Delta f}{f_r})(n_s/n_B) \qquad (16a)$$

or

$$\text{SNI} = \frac{1}{4\Delta f}\sqrt{\frac{\eta n_B}{t_r \tau}} \qquad (16b)$$

For the conditions examined, namely $\Delta f = 10^7$ Hz, $\eta = 0.04$, $n_B \approx 10^4$, $t_r \approx 15(10^{-9})$ sec and $\tau = 800(10^{-9})$, the SNI is predicted to be only about 5, approximately that experimentally determined. The large filter bandwidth, Δf, is necessitated by the short laser pulse duration. Note also that the SNI is dependent on the absolute noise level. For larger n_B, the PMT shot noise is correspondingly a smaller fraction of the absolute noise signal and is better suppressed by the filtering. In Raman work where the photon yields are small, typically 10^3-10^4 photons per pulse, low S/N ratios still engender low noise photon levels. The aforementioned technique

would be quite useful for polarization sensitive processes where the photon yields are much greater. For example, if $n_s = 10^7$ and $n_B = 10^8$, an initial S/N of .1, the SNI using the modulation technique would be 500, resulting in a S/N after filtering of 50. Although the SNI could be further increased via phase sensitive detection with a long time constant and subsequent averaging, this approach with its more complicated apparatus does not offer any advantage over the simpler noise sampling and subtraction schemes previously discussed.

LASER IRRADIATED PARTICULATE NOISE SCALING

The goal of this portion of the experimental program is aimed at investigating the validity of the previously described analysis which predicted a relatively weak dependence of particle surface temperature with laser flux level. This, in turn, led to the predicted S/N improvements with increasing focal flux displayed in Table III. In the following portions of this section, the interaction of particulates with laser radiation will be discussed, various seeding approaches will be reviewed, those chosen described and the experimental results obtained will be presented.

Interaction of Particulates with Laser Radiation

The absorption of laser radiation by the particulates will be considered following the treatment developed in Ref. 19 concerning the effects of aerosol particle heating on laser beam propagation.

The absorption cross-section, σ_a, of particles with radius a is assumed to behave as

$$\sigma_a = \beta(n)\pi a^2 \quad a > \delta \qquad \sigma_a = \beta(n)\frac{\pi a^3}{\delta} \quad a < \delta \tag{17}$$

where δ is an absorption length parameter to be evaluated subsequently. $\beta(n)$ is a function of the index of refraction which accounts for radiation reflection off the particle surface, and for carbon, is about 0.9. More exactly δ is given by the expression

$$\frac{1}{\delta} = 2kn_1 \left\{ \frac{12 n_o \beta^{-1}(n)}{4 n_o^2 n_1^2 + (n_o^2 - n_1^2 + 2)^2} \right\} \tag{18}$$

where $n = n_o - in_i$ is the complex index of refraction, and k, the wave vector, $2\pi/\lambda$. The optical constants of soot have been measured (Ref. 20) and are not critically dependent on the hydrogen/carbon ratio. At 550 nm (the laser "line" is approximately 587 nm), $n_o = 1.56$ and $n_i = 0.46$. Inserting these values in Eq. (6) gives a value for δ of 0.1μ. For carbon particulates (soot) larger than 0.1μ, laser absorption is essentially geometric while for smaller particles the absorption is less than geometric by the factor a/δ. In the previously displayed (Fig. 4) laser irradiated particle heating results, the dependence of the absorption cross section with particle size was taken into account in preparing the heat conduction curves. Although simulations of laser induced combustor noise had been performed with Arizona natural dust (Ref. 21), it is clear from Eq. 18 that attention be directed to the refractive index constants of any proposed seed. For example, alumina particles come in well controlled size ranges and might appear attractive for seeding purposes. However, alumina possesses an imaginary refractive index component of 10^{-6} in the visible (δ very large in Eq. (18)) so that the visible absorption coefficient varies from 10^{-5} to 10^{-4} times the geometric cross section for particles in the 0.1 to 1.0μ range respectively (Ref. 22). Consequently, very little incident energy is absorbed by an alumina particle, and little heating occurs unlike the situation with carbonacious particles. Furthermore, the emissivity of alumina is a factor of two to three lower than that for carbon (Ref. 23), leading to reduced radiative output for whatever heating does occur. Hence, it is not surprising that the purposive introduction of alumina particles has had little effect on laser Raman diagnostic accuracy (Ref. 24). In fact, alumina particles are an excellent seed for

simultaneous LDV - laser Raman work since laser induced, alumina incandescent noise should be quite small.

Seeding Approaches

It is clear from the foregoing discussion that if one wishes to study laser induced particulate noise from combustion generated soot, then carbonacious seeds should be employed. Preliminary tests with simple, air convective seeders proved them to be temporally irreproducible and unsteady. Discussions with colleagues experienced in seeding indicated this could be a very time consuming avenue of approach. A soot generator similar to that of Ref. 25 but without a heated chimney was fabricated and also found to be temporally unsteady due to nozzle unclogging and clogging. To avoid these difficulties and in an attempt to obtain reproducible data, it was decided to irradiate singly suspended particles in an already existing particle suspension apparatus available in the laboratory. With this apparatus which will be described subsequently, particles 5μ in diameter and larger could be suspended. During the course of these experiments, particle sizing measurements (Ref. 26) made on the previously described combustor (Fig. 2) approximately 1.5 m downstream from the fuel injection location revealed an average particle size of approximately 0.04μ at a number density of 7×10^{8} cm^{-3}. Due to the size sensitivity of particle surface temperature at modest flux levels, these particle suspension experiments were terminated due to the large particle constraint of the apparatus. Since laminar, hydrocarbon-fueled, diffusion flames are known (Ref. 27, 28) to produce soot in the size and density ranges measured above, it was decided to study

the scaling of laser induced particulate noise in such flames. Before proceeding to discuss the results of these studies, the singly suspended, laser irradiated particle studies will be briefly reviewed.

Singly Suspended Particle Studies

Figure 7 schematically depicts the arrangement employed for the laser irradiated, singly suspended particle studies. The individual particles were suspended electrodynamically in a cubical electrode array in a manner detailed in Refs. 29, 30. Copper electrodes, 5 cm in diam with a 2.5 cm aperture, arranged in a cube 6.3 cm on a side were housed in a plexiglas container fixed with pyrex viewing and irradiation windows. Carbon particles placed in a reservoir drop through a 400 mesh screen and pass through a positive corona discharge apparatus atop the plexiglas container. The electrically charged particles then enter into the cubical electrode volume and orbit in the fields. Minimum orbit diameters are on the order of 100μ. The particles are viewed by a 10x microscope and positioned in the focus of a helium-neon laser beam of approximately 150μ diameter by appropriate dc voltage adjustment. The minimum dye laser focal diameter is about 700μ and, hence, the above procedure permits accurate centering of the focussed dye laser beam on the particle. The laser induced particle radiation is monitored on the two channel Raman spectrometer which for these studies functions as a two color pyrometer. For these studies the spectrometer was calibrated against a blackbody source at 1258^{o}K.

Initial studies employed Union Carbide graphite #38, guaranteed at 98.5% less than 200 mesh. The graphite was further sieved through 400 mesh prior to placing it in the reservoir. Absolute particle radiation levels tended to be irreproducible presumably due to lack of particle size control from shot to shot, i.e., the particles were simply less than 40μ. Much more reproducible behavior was obtained using a "5μ" graphite powder from Consolidated Astronautics.

Quite interestingly, the relative radiation levels at 5169Å and 6811Å (the filters used for detecting the vibrational Raman from N_2 for excitation at 5877Å) did not correspond to the Planck radiation law at any temperature, except for the smallest flux levels studied ($< 10^6$ W/cm^2). Even when "temperatures" were obtained, they were far above those predicted in Fig. 4. Assuming an excess amount of radiation at 5169Å, it appears Swan band emission from C_2, a major vaporization product (Ref. 31), is being detected in addition to incandescence. The Raman anti-Stokes N_2 filter at 5169Å would include the (0,0) Swan band head at 5165Å. There are numerous cases in the literature (Refs. 32, 33, 34) where C_2 Swan band radiation has been excited in ruby laser irradiated graphite studies. In Fig. 8, the Swan spectrum produced from a 0.3 cm dia graphite rod irradiated with dye laser radiation at 5950Å is shown. Note the strong (0,0) band at 5165Å.

With the advantage of tunability, the Swan bands can be avoided with a dye laser appropriately tuned. For the diffusion flame data to be reported subsequently, the laser was retuned to 5917Å placing the N_2 Raman Q branches at 5200Å and 6864Å. Note that around 5200Å, there is a Swan band "window." Unfortunately, fixed frequency

lasers are not so flexible. Table IV shows that Swan interferences from laser irradiated soot may be present for N_2 Raman studies using either ruby or frequency-doubled YAG lasers.

TABLE IV

Potential Laser Raman Swan Interferences

Laser, Wavelength	Q Branch N_2 Raman Wavelength, Angstroms	Swan Band
Ruby, 6943	8284	-----
	5976	6004.9 (3,5)
		5958.7 (4,6)
2x Nd:YAG, 5320	6073	6122.1 (1,3)
		6059.7 (2,4)
	4733	4737.1 (1,0)

Laser induced Swan band emissions have also been produced from combustion generated soot as will be seen in the next section.

Laminar Diffusion Flame Studies

To simulate the soot sizes measured in the Fig. 2 combustor, the majority of the laser irradiated particulate "noise" studies were conducted on laminar propane or methane diffusion flames. These were stabilized on a stainless steel tube 0.64 cm in outer diameter with a 0.48 cm bore. These tubular diffusion flames are very similar in appearance to candle flames as seen in Fig. 9. To ensure spatial stability of the flame, the tube was housed in a 6 armed glass cross. The four horizontal arms were fitted with pyrex windows for laser irradiation and viewing. The upper arm was open; the lower arm elevated slightly off of the base support

to avoid oxygen starvation. The data from these flames are quite reproducible as shown in Fig. 10 where a triple trace overlay is displayed of the laser modulated particulate incandescence in an ~ 11Å bandwidth centered at 5230Å and 6864Å. The laser induced noise levels in these flames are very high; the (Raman signal)/(laser induced particulate noise) is typically below 10^{-4} when propane is used. Neutral density filters were used to attenuate the laser induced noise prior to detection by the Raman spectrometer.

The spectral radiant emittance (radiant power per unit area per unit wavelength interval) is given by the Planck radiation formula

$$W_\lambda = \frac{2\pi c^2 h}{\lambda^5 (e^{hc/\lambda kT} - 1)} \epsilon_\lambda \qquad (19)$$

where h is Planck's constant; c, the speed of light; k, Boltzmann's constant; T, temperature, and ϵ_λ the emissivity, which is assumed to be roughly constant between 5000 and 7000Å (Ref. 35). If the laser induced incandescence is monitored at the anti-Stokes, λ_A, and Stokes, λ_S wavelengths, then particle surface temperature may be obtained from the relation

$$T = \frac{\frac{hc}{k}\left(\frac{1}{\lambda_S} - \frac{1}{\lambda_A}\right)}{5 \ln \frac{\lambda_A}{\lambda_S} + \ln \frac{W_A}{W_S}} \qquad (20)$$

Naturally one monitors the photomultiplier tube output which is related to energy received via the collection efficiency of the Raman spectrometer, the tube sensitivity and gain. Actually only the ratio of these factors for the two spectral regions of interest is required and this is readily obtained from a blackbody calibration. In the present experiments, the spectrometer was calibrated against a tungsten

filament whose brightness temperature was measured with a calibrated optical pyrometer. The spectral variation of the emissivity of tungsten is well known (Ref. 23) permitting the actual filament temperature to be ascertained. Thus from data similar to that of Fig. 10, particulate temperatures can be ascertained as a function of laser flux level.

In Fig. 11, the measured particle surface temperatures as a function of peak laser focal flux level are shown. The particulate incandescence was monitored at 5230Å and 6864Å to avoid Swan band radiations. The data were generated by varying both the focal length of the focussing lens and the laser pulse energy as shown by the varying symbols. The focal fluxes were experimentally determined by measuring the energy transmitted through varying size apertures at the lens focus. The flame was irradiated about 1.3 cm above the tube end, approximately half of the flame height. The spread in the data points at any given focal flux is indicative of the apparent measurement error, approximately ± 10%. Also shown is the temperature-focal flux dependence (dotted) predicted by the quasi-steady laser irradiated particle heating analysis. The agreement between the analysis and the experiment is fairly good. The data point at the lowest focal flux would be expected to be at a considerably lower temperature as seen since, for particle sizes prevailing in the flame, heat conduction should be important at the lower flux level (Fig. 4). Particle sizes and number densities were determined for the flame using a Mie scattering/absorption technique. To increase the absorption path length, a specially constructed burner consisting of eight aligned tubes was constructed. These measure-

ments indicated an average particle diameter of about 0.04μ and a soot density of $4(10^{10})$ cm^{-3}. Recall that similar measurements in the Fig. 2 combustor indicated roughly the same particle size and a density of 7×10^{8} cm^{-3}; hence, good size simulation was obtained. The absolute number density level affects only the magnitude of the laser induced noise generated.

A series of flame temperature measurements shown in Fig. 12 was made using the 5169, 6811Å filters. Not surprising with this filter set, the measured "temperatures" are quite high at the higher laser fluxes, due presumably to Swan emissions from C_2 contributing to the radiation under the 5169Å filter, leading to abnormally high W_A/W_S ratios. At the flux levels above 10^{7} W/cm^2, W_A/W_S is so high that Eq. (20) yields negative temperatures.

Of more immediate importance, of course, is the scaling of the absolute noise level. In Fig. 13, the absolute noise level (arbitrary units) is shown as a function of laser pulse energy with focussing lens focal length shown parametrically. Recall that the Raman scattering is solely energy (not flux) dependent. As can be seen, the noise after rising sharply in the 1-60 mJ energy range, becomes nearly constant thereafter, and decreases with decreasing focal length. The highest energy data points, where the noise is somewhat lower (by 15-30%) than that at lower energies, were obtained during a different experimental run and reflect the difficulty of reproducing accurately the absolute noise levels. Since there is no obvious physical reason for the noise to decrease with increasing energy, the curves have been drawn flat. Aperture losses prevented obtainment of the higher energies with the shortest focal length lens.

The behavior shown in Fig. 13 arises for two reasons: Firstly, the smaller focal length lenses lead to smaller focal diameters resulting in fewer particulates being irradiated by the Raman inducing laser pulse. Secondly, for focal fluxes above a few megawatts/cm^2 vaporization dominates the heat transfer for the small particles in the flame (Fig. 4) leading to the fairly flat temperature behavior shown in Fig. 11. As the energy increases, the particulate temperatures increase only gradually leading to the fairly flat variations of noise with energy seen. Despite the higher surface temperatures at low energies, which result from the smaller focal length lenses, the absolute noise levels for the various focal lengths are comparable at low energy due to the decrease in the number of particles irradiated with shorter focal lengths.

From Fig. 13, the SNI (signal/noise improvement) for the varying focal length lenses can be determined. For example, for the 40 cm focal length lens the Stokes noise increases from 3 to 10 for an energy increase from 6 mJ (corresponding to a flux of $2(10^5)W/cm^2$) to 300 mJ, a SNI of about 15. A comparable SNI results by switching from the 40 cm lens to the 10 cm lens, but for a smaller increase in energy, i.e., to 90 mJ. Assuming the noise continues to exhibit the flat behavior for the 10 cm focal length lens, for slightly over an order of magnitude increase in energy to 1.8 J (a focal flux of $\sim 10^9$ W/cm^2), the SNI would be on the order of 300. This is less than that predicted in Table III, and probably results from the fact that experimentally one does not have a uniform focal flux distribution. About 20% of the laser energy at the focal point resides in poorly focussed wings. Consequently, the outer

regions of the focal spot, possessing considerably lower flux levels, do not heat the particles as strongly as the central region leading to a washing out of the stronger scaling predicted. Nevertheless, the results clearly indicate the S/N advantages to be gained from operation at high focal flux levels. In general then, in sooting flames one should operate at the highest flux levels possible, short of the gas breakdown threshold, of course.

High Focal Flux Problems

Other than the obvious problem of gas breakdown, operation at high focal fluxes can lead to other, perhaps less apparent problems. For small scale research combustors, high focal flux levels generally lead to high flux levels passing through the optical ports of the device. In Raman tests on the Fig. 2 combustor with a ruby laser operating at about half a joule in 30 nanoseconds, window breakdown occurred for focussing focal lengths less than 70 cm even in schlieren grade quartz windows.

Another problem encountered on the Fig. 2 combustor using a dye laser was window fluorescence which led to noise interferences on the Stokes Raman channel. This occurred for flux levels through the window on the order of 10^6 watts/cm^2. Although the fluorescent noise was easily circumvented by observing the Raman scattering at right angles, right angle viewing usually leads to higher luminous background noise levels for the optical collection system shown in Fig. 1. This arises due to the larger sampling volume that right angle viewing engenders relative to coaxial viewing. This is illustrated in Fig. 14. With unity magnification in the primary collection lens system, the Raman sampling extent at right angles is determined by and is equal

to the aperture opening A. However, all background light within the depth of field of the optical system will be seen by the spectrometer. The depth of field is approximately $2fA/D$, where f and D are, respectively, the focal length and diameter of the collection lens. The total sampling volume is $(\pi/2)f'A^3$, where f' is the f number of the lens system, i.e., f/D. With coaxial collection, i.e., backscattering, the aperture A can be significantly reduced since the Raman sampling extent is aligned with the depth of field. For equivalent Raman sampling extents and an f/3 lens system the aperture opening A for coaxial scattering can be made a factor of six smaller than that for right angle viewing, leading to a reduction in sampling volume of 216. This is an extremely important consideration particularly when attempting measurements in the luminous environments characteristic of many practical combustion situations. With right angle viewing, the (Raman signal)/(natural background luminosity noise) ratio in the primary zone of the Fig. 2 combustor burning propane was below 10^{-2} precluding Raman measurements. Special window designs may prevent detection of the fluorescence and permit use of coaxial viewing schemes. Designs involving compound windows with opaque barriers may not be trivial to implement, however, for work in combustors where the window temperature may well exceed $1000^{\circ}K$.

SIGNAL AVERAGING CONSIDERATIONS

In Ref. 3, Setchell has examined the consequences of time-averaging Raman data generated by a cw laser from a turbulent medium. In this section we will consider the case when pulsed laser Raman data needs to be ensemble-averaged in a fluctuating environment and the consequences of such averaging. Ideally with a pulsed laser of sufficiently short duration, "instantaneous" temperature measurements can be made. Realistically, however, the Raman S/N is often limited by shot noise and background noise (naturally occurring or laser induced) and signal averaging is required prior to further treatment of the data. The question naturally arises then as to what one has actually "measured" after such averaging operations. First, we begin in an introductory vein with the case of ensemble averaging Raman data with no shot or background noise. This will be followed by extensions of the analysis incorporating these effects.

No Background, No Shot Noise

In the following, the laser pulse energy will be assumed to be constant from pulse to pulse and will not be explicitly considered. If desired it can be treated in a manner analogous to the shot noise treatment of the next section. The number of Raman photons n_i^s (s, Stokes band; later the superscript a will be used to denote the anti-Stokes region) generated by the ith pulse is given by

$$n_i^s = k^s n_i f^s(T_i) \tag{21}$$

where n_i is the number density of the scattering species at instant i and $f^s(T_i)$,

the bandwidth factor, a temperature dependent term which accounts for the fraction of the scattering species in the appropriate initial quantum states for scattering to be observed. $f^s(T_i)$ is bandwidth sensitive and depends on the spectral location and bandwidth of the spectrometer or interference filters employed; this dependence is not explicitly denoted in the analysis. k^s is a factor dependent on geometry, collection efficiency of the optical system and laser pulse energy, and is assumed constant. The number of Stokes photoelectrons, S_i, generated by the Stokes photomultiplier tube is

$$S_i = \eta^s n_i^s = \eta^s k^s n_i f^s(T_i) \tag{22}$$

where η^s is the tube quantum efficiency at the Stokes wavelength. It is assumed here that the shot noise variation, $\sim\sqrt{\eta n_i^s}$, on the signal is tolerably small. The analysis in the following section will treat the case when this is not so. Similar relations apply to the anti-Stokes scattering. The anti-Stokes to Stokes ratio at any instant is solely temperature dependent

$$R_i = \frac{A_i}{S_i} = \frac{\eta^a k^a f^a(T_i)}{\eta^s k^s f^s(T_i)} \tag{23}$$

permitting T_i to be measured. In Fig. 15, f^a, f^s, f^a/f^s are displayed as a function of temperature for conditions typical of those used for temperature measurements. The average temperature $\bar{T}$ (where bars are used here to denote ensemble and not time averages) is obtained from

$$\bar{T} = \frac{1}{N} \sum_{i=1}^{N} T_i \tag{24}$$

where N represents a statistically significant sample size. It should be noted that

in general $\bar{T}$ is not obtained from $\bar{R}$. Expanding R_i is a power series about $\bar{T}$,

$$R_i = R(T_i) = R(\bar{T}) + \frac{dR(\bar{T})}{dT} T_i' + \frac{1}{2} \frac{d^2R(\bar{T})}{dT^2} T_i'^2 \qquad (25)$$

where $T_i = \bar{T} + T_i'$, where T_i' is the deviation of temperature at any instant from the mean, we see upon averaging that

$$\bar{R} = R(\bar{T}) + \frac{1}{2} \frac{d^2R(\bar{T})}{dT^2} \overline{T_i'^2} \qquad (26)$$

Only in those cases where R is a linear function of T does $\bar{R} = R(\bar{T})$. In some temperature regions and with proper choice of bandwidth, R can be made to behave nearly linear with temperature (Refs. 1, 3, 4) as seen in Fig. 15, permitting the average temperature to be obtained from $\bar{R}$ if the temperature fluctuations are not too large. The error in mean temperature using $\bar{R}$ can be determined by expanding T in a series about R_o, where $R_o \equiv R(\bar{T})$

$$T(\bar{R}) = T(R_o) + \frac{dT(R_o)}{dR} (\bar{R} - R_o) + \frac{1}{2} \frac{d^2T(R_o)}{dR^2} (\bar{R} - R_o)^2 + \ldots \qquad (27)$$

where $T(R_o) \equiv \bar{T}$. Inserting $\bar{R} - R_o$ from (26), one obtains

$$T(\bar{R}) - \bar{T} = \frac{1}{2} \frac{dT(R_o)}{dR} \frac{d^2R(\bar{T})}{dT^2} \overline{T_i'^2} + \frac{1}{8} \frac{d^2T(R_o)}{dT^2} \left(\frac{d^2R(\bar{T})}{dT^2}\right)^2 \overline{T_i'^2} \qquad (27)$$

Using Eq. (28) one can estimate the error in mean temperature resulting from using $\bar{R}$ in a fluctuating medium with mean square temperature fluctuations of a given magnitude since all of the derivatives in Eq. (28) are calculable.

It is also important to note that one does not obtain the average temperature from a measurement of $\bar{A}/\bar{S}$, i.e., the case where the anti-Stokes and Stokes signals are separately averaged, then ratioed. The average Stokes signal is

$$\bar{S} = \frac{1}{N} \sum_{i=1}^{N} S_i = \frac{\eta^s k^s}{N} \sum_{i=1}^{N} n_i f^s(T_i) \tag{29}$$

Expressing n_i and $f^s(T_i)$ in terms of mean and fluctuating quantities

$$n_i = \bar{n} + n_i' \qquad f^s(T_i) = \overline{f^s(T)} + f^{s\,\prime}(T_i) \qquad \text{where } \overline{f^s(T)} \neq f^s(\bar{T}) \tag{30}$$

where $\overline{n_i'} = 0$, and $\overline{f^{s\,\prime}(T_i)} = 0$, and expanding $f^s(T_i)$ about $\bar{T}$

$$f^s(T_i) = f^s(\bar{T}) + \frac{df^s(\bar{T})}{dT} T_i' + \frac{1}{2} \frac{d^2 f^s(\bar{T})}{dT^2} T_i'^2 \tag{31}$$

one can show that Eq. (29) becomes

$$\bar{S} = \eta^s k^s \left[\bar{n} f^s(\bar{T}) + \overline{n'T'} \frac{df^s(\bar{T})}{dT} + \frac{1}{2} \frac{d^2 f^s(\bar{T})}{dT^2} \left(\overline{\bar{n}T'^2} + \overline{n'T'^2} \right) \right] \tag{32}$$

A similar relation pertains to the anti-Stokes photoelectrons. Hence, $\bar{A}/\bar{S}$ is not a function solely of $\bar{T}$, but also of $\bar{n}$, $\overline{n'T'}$, $\overline{n'T'^2}$, and $\overline{T'^2}$, the magnitudes and correlations of the fluctuations.

If the Stokes filter is made sufficiently broad (on the order of 50Å for N_2 and laser excitation at 5900Å), then the bandwidth factor, $f^s(T)$ = constant, and $\bar{A}/\bar{S}$ becomes

$$\frac{\bar{A}}{\bar{S}} = \frac{\eta^a k^a}{\eta^s k^s f^s(T)} \left[f^a(\bar{T}) + \frac{\overline{n'T'}}{\bar{n}} \frac{df^a(\bar{T})}{dT} + \frac{1}{2} \frac{d^2 f^a(\bar{T})}{dT^2} \left(\overline{T'^2} + \frac{\overline{n'T'^2}}{\bar{n}} \right) \right] \tag{33}$$

where generally $\frac{df^a}{dT} > 0$, and $\frac{d^2 f^a}{dT^2} < 0$ due to the exponential growth of vibrational anti-Stokes scattering with temperature. The last two terms in Eq. (33) tend to cancel, the degree to which depends on the magnitude and correlation of the density and temperature fluctuations. It is well to point out that the fluctuations in a primary turbulent combustion zone could be quite large. At various time instants

one could be probing a spectrum of conditions ranging from cool unreacted gases to hot reacting combustion products. The analysis just presented, however, is restricted to small and moderate fluctuations, since very large fluctuations in density and temperature would invalidate the limited series expansions employed.

No Background, Shot Noise

As mentioned, Eq. (22) pertains only to the case where the photomultiplier shot noise is sufficiently small to permit S_i to be acquired to some desired precision independent of the shot noise variations. This, of course, is not often the case with Raman diagnostics. For example, if 1000 Raman photons are detected with a tube possessing a 10% quantum efficiency, the signal would typically exhibit variations about the mean of ± 10%. Since the photon detection process is statistical, the number of photoelectrons generated by any one pulse is indeterminate, and is accounted for in the previous analysis by inserting a factor m_i into Eq. (22)

$$S_i = k^s \eta^s m_i{}^s n_i f^s(T_i) \tag{34}$$

Fluctuations in laser pulse energy from shot to shot could also be accounted for using such a factor. $m_i{}^s$ will vary about unity with a Poisson distribution (Ref. 17) and can be written as

$$m_i{}^s = 1 + m_i{}^{s'} \tag{35}$$

One now proceeds in a manner analogous to that of the last section. Since the medium fluctuations (n', T') are statistically independent (i.e., uncorrelated) of the photomultiplier shot noise variations, terms such as $\overline{m_i{}^{s'} n_i{}'}$ are separable (Refs. 36)

to $\overline{m_i^{s'} n_i'}$ and vanish. If the Stokes and anti-Stokes channels are separately averaged all of the shot noise terms go to zero for suitably long averaging and Eq. 32 again results. As before $\bar{A}/\bar{S}$ depends on the magnitude and correlation of the fluctuations and not solely on average temperature.

If the A_i/S_i ratio is formed first, number density again cancels and one makes a "temperature" measurement from the ratio

$$R_i = \frac{k^a \eta^a f^a(T_i) m_i^a}{k^s \eta^s f^s(T_i) m_i^s} \tag{36}$$

with some error due to the shot noise term, m_i^a/m_i^s. Intuitively one might suspect these temperature measurement errors to cancel out over a large sample of measurements. We will show that in general this is not the case. Consider the case of a laminar flame with constant (in time) temperature $\bar{T}$ at the measurement location. The ratio corresponding to this temperature is denoted by R_o, $T(R_o) \equiv \bar{T}$, as before. The measured ratio R_i will vary from R_o on each shot due to the shot noise fluctuations

$$R_i = R_o \frac{m_i^a}{m_i^s} = R_o + R_i' \tag{37}$$

Turbulent flame situations can be handled by adding another multiplicative factor to the $R_o\ m_i^a/m_i^s$ term to account for temperature fluctuations about the mean. For simplicity we will examine the laminar flame case only. The error in measured temperature from the true temperature can be obtained by expanding T about R_o

$$T(R_i) = T(R_o) + \frac{dT(R_o)}{dR} R_i' + \frac{1}{2} \frac{d^2T(R_o)}{dR^2} R_i'^2 \tag{38}$$

Expressing m_i^a, m_i^s as in Eq. (35), and expanding m_i^a/m_i^s, R_i' can be shown to be

$$R_i' = R_o(m_i^{a'} - m_i^{s'} - m_i^{s'} m_i^{a'}) \tag{39}$$

Substituting Eq. (39) into (38) and averaging, we obtain

$$\overline{T(R)} = \bar{T} + \frac{1}{2}\frac{d^2T(R_o)}{dR^2} R_o^2 \left(\overline{m^{a,2}} + \overline{m^{s,2}} + \overline{m^{a,2} m^{s,2}} \right) \qquad (40)$$

showing that the shot noise fluctuations (or fluctuations in laser energy) do not average out but lead to an error in mean temperature for a non-zero second derivative. For Poisson distributed shot noise, the $\overline{m'^2}$ terms can be shown to be

$$\overline{m'^2} = \frac{1}{\eta \bar{n}} \qquad (41)$$

where $\bar{n}$ is the average number of photons collected per pulse. The third term in the brackets in Eq. (40) is separable due to the statistical independence of the shot noise on different photomultiplier tubes.

Background Subtraction

Consider now the situation where, in addition to the Raman signal, there are sources of noise, either naturally occurring or laser induced, present in the "signal." The number of Stokes photoelectrons is then

$$S_i = \eta^s (n_i^s + n_i^{sn})\, m_i^s \qquad (42)$$

where n_i^{sn} are the number of noise photons in the Stokes bandpass. If another channel is placed in a spectral region adjacent to the Raman spectrum, the noise can be sampled assuming that it is fairly smooth spectrally. This is generally the case for laser induced or naturally occurring soot incandescence. The noise channel will deliver SN_i photoelectrons

$$SN_i = \eta^s n_i^{sn} m_i^{sn} \qquad (43)$$

where for simplicity the quantum efficiency is considered to be the same for each tube. The desired "signal" is obtained by subtracting the Stokes noise channel from the Stokes channel with the result

$$\mathscr{S}_i = S_i - SN_i = \eta^s n_i^s m_i^s + \eta^s n_i^{sn}(m_i^s - m_i^{sn}) \tag{44}$$

the subtraction being imperfect due to the accompanying shot noise on each tube. Figure 5 displays typical subtraction accuracies pertaining on the average; as Eq. 44 shows on any one shot the situation could be better or worse depending on the exact nature of the shot noise fluctuations. Upon sufficient signal averaging, Eq. (44) becomes

$$\bar{S} = \eta^s \overline{n_i^s m_i^s} + \eta^s \left(\overline{n_i^{sn} m_i^s} - \overline{n_i^{sn} m_i^{sn}} \right) \tag{45}$$

Due to the statistical independence of the shot noise and the signal or noise photons the $\overline{nm}$ terms are separable, and recalling that $\bar{m} = 1$, we obtain

$$\bar{\mathscr{S}} = \eta^s \overline{n^s} = \eta^s k^s \left[\bar{n} f^s(\bar{T}) + \overline{n'T'} \frac{df^s(\bar{T})}{dT} + \frac{1}{2} \frac{d^2 f^s(\bar{T})}{dT^2} \left(\overline{nT'^2} + \overline{n'T'^2} \right) \right] \tag{46}$$

as before. In the above we have assumed that the variations in n_i^{sn} from shot to shot are not large enough to cause m_i^{sn} and n_i^{sn} to be correlated. Although $\bar{\mathscr{A}}/\bar{\mathscr{P}}$ (where $\mathscr{A}_i = A_i - AN_i$) is independent of background and shot noise effects, the previously described situation pertains, namely that $\bar{\mathscr{A}}/\bar{\mathscr{P}}$ is not dependent on average temperature alone but also on the magnitudes and correlations of the fluctuations.

If the $\mathscr{A}_i/\mathscr{S}_i$ ratio is first formed, one obtains

$$\frac{\mathscr{A}_i}{\mathscr{S}_i} = \frac{\eta^a k^a n_i f^a(T_i) m_i^a + \eta^a n_i^{an}(m_i^a - m_i^{an})}{\eta^s k^s n_i f^s(T_i) m_i^s + \eta^s n_i^{sn}(m_i^s - m_i^{sn})} \tag{47}$$

somewhat intractable to further analysis. The situation can be handled by expressing $\mathcal{A}_i$, $\mathcal{S}_i$ as

$$\mathcal{S}_i = \eta^s n_i^s m_i^s + RE \frac{\eta^s n_i^{sn} (m_i^s - m_i^{sn})}{\eta^s n_i^s m_i^s} \tag{48}$$

where RE denotes the relative error which can be positive or negative depending on the sign of $m_i^s - m_i^{sn}$. Thus $\mathcal{A}_i/\mathcal{S}_i$ may be written

$$R_i = \frac{\mathcal{A}_i}{\mathcal{S}_i} = \frac{\eta^a n_i^a m_i^a}{\eta^s n_i^s m_i^s} + \frac{\eta^a n_i^a m_i^a}{\eta^s n_i^s m_i^s} \left(\frac{n_i^{an} (m_i^a - m_i^{an})}{n_i^a m_i^a} + \frac{n_i^{sn} (m_i^s - m_i^{sn})}{n_i^s m_i^s} \right) \tag{49}$$

The situation is still intractable except to note that Eq. (49) after some manipulation can be used to define an R_i' as in Eq. (37). There it was shown that the errors in a set of "instantaneous" "temperature" measurements would not average out and that an erroneous average temperature would result, Eq. (40), for a nonzero second derivative of R with temperature. Here an erroneous temperature measurement will result with each laser pulse except for the rare instance when the shot noise fluctuations on the four tubes are the same. The average measured temperature will depart from the time average (averaging Eq. 38))

$$\overline{T(R_i)} - \bar{T} = \frac{dT(R_o)}{dR} \overline{R_i'} + \frac{1}{2} \frac{d^2 T(R_o)}{dR^2} \overline{R_i'^2} \tag{50}$$

depending upon the magnitudes of $\overline{R_i'}$ and $\overline{R_i'^2}$. The latter in turn will be dependent on the signal and noise levels in a particular situation.

Implications of Signal Averaging

There are a number of conclusions which can be drawn from the foregoing analyses. First, in measurement situations where the anti-Stokes to Stokes ratio cannot be determined to a high level of accuracy, the temperature measured at each instant will, of course, be erroneous. Quite importantly, the average of these erroneous measurements will not yield the true average temperature, but will depart from it depending on the magnitude of the gasdynamic and shot noise fluctuations. Second, these errors can be eliminated or reduced if, by manipulation of spectral bandwidths and center frequencies, the anti-Stokes/Stokes ratio is made a linear function of temperature over the "temperature" range of interest. By "temperature" range is meant the temperature inferred from the measured anti-Stokes to Stokes ratio; this range may well be considerably larger than the actual physical temperature range. The linearity in the ratio variation with temperature will cause the second derivative terms $d^2T(R_o)/dR^2$ and $d^2R(\bar{T})/dT^2$ to vanish or be negligibly small in many of the previous expressions. Third, when the anti-Stokes and Stokes data are separately averaged, background can be subtracted on average and shot noise terms will average to zero. However, the temperature inferred from the ratio of averaged anti-Stokes to averaged Stokes will also not be the average temperature, but will vary depending upon the magnitude and correlations of the fluctuations.

SEEDED FLAME TEMPERATURE MEASUREMENTS

Although the advantages (in terms of S/N) of operating at high focal flux levels have been demonstrated in an earlier section, measurement situations are likely to be encountered, where, despite the use of high focal fluxes, the S/N will be low enough to preclude accurate Raman measurements. For example, in the previously described propane diffusion flame studies, the S/N at moderate focal flux, 10^6 W/cm^2, was less than 10^{-4}. Operation at flux levels near 10^9 W/cm^2 would lead to extrapolated improvements in S/N to somewhat above 10^{-2}, a still intractable measurement situation. In those instances where the noise cannot simply be overpowered by signal, additional steps need be taken to account for or eliminate the noise. The inadequacy of the Raman amplitude modulation approach for noise suppression was previously described. Hence, noise sampling and subtraction appears to be the only alternative for spontaneous Raman work in high "noise" environments. As seen previously, due to the shot noise behavior of photomultipliers, subtraction cannot be performed accurately for an individual pulse, but only on average for a large number of pulses. Averaging, in turn, leads to a situation where the ratio of the averaged anti-Stokes to averaged Stokes signals depend not on average temperature alone, but also on the magnitude and correlation of the medium fluctuations as well. Further study is required to ascertain the severity of these effects on Raman measurement accuracy.

To investigate the feasibility of noise sampling and subtraction, a flat flame burner was constructed with provision to introduce a controlled amount of laser induced particulate incandescent noise. The Raman spectrometer was operated in a

four channel mode (two noise and two signal) and "temperature" measurements were performed with and without the seed in a manner to be described shortly. Before proceeding to that, some clean flame temperature measurements will be described together with a short discussion of Raman temperature measurement accuracy with narrow ($\sim 10\text{Å}$) filter bandwidths.

Clean Flame Temperature Measurements

Raman temperature measurements were performed with the Raman spectrometer in the two channel mode (Fig. 1) but at right angles to the laser beam. Measurements were performed on a 7.6 cm dia. flat flame burner operating on air and methane at an equivalence ratio of about 0.7. The measurement volume was cylindrical in shape with an axial extent of 5 mm and a diameter of 1.5 mm. Because the spectrometer was very polarization sensitive due to the dichroic, measurements and calibrations were performed with a polarization filter in the spectrometer after the small collimating lens. The Raman signals were recorded on an oscilloscope and averaged on film. Leakage currents on our signal averager were too high to permit accurate utilization of the instrument at the low pulse rate, 1 pps, of our dye laser. Typical data are shown in Fig. 16 where the Raman scattering in room air and in the flame is displayed. The flame data represents about 20 pulses overlaid. Variations from shot to shot are primarily due to shot noise. These were minimized by integrating the signals with a time constant comparable to the laser pulse duration, thus sampling in essence the total number of photoelectrons produced. For example, based on an absolute photo-

multiplier tube calibration made with a tungsten filament lamp, the flame Stokes signal corresponds to about 500 photons, which for the 4% quantum efficiency of the tube at the Stokes wavelength, results in a predicted shot noise fluctuation of ± 25%, approximately that seen.

Temperature can be extracted from the Fig. 16 data in two ways as shown in Fig. 17, either from the anti-Stokes to Stokes ratio or Stokes to Stokes ($300^{\circ}K$) ratio. To relate the voltage ratio experimentally measured to the energy ratio derived as a function of temperature from the computer code (Appendix II) a calibration is performed with a tungsten filament whose brightness temperature is measured with an optical pyrometer. The brightness temperature is then corrected to actual filament temperature based on the transmissivity of the glass envelope on the filament lamp and the known emissivity of tungsten as a function of temperature and wavelength (Ref. 23). The anti-Stokes to Stokes ratio shown in Fig. 16 resulted in a temperature of $1675^{\circ}K$. Other trials resulted in temperatures of $1620^{\circ}K$, $1660^{\circ}K$ and $1615^{\circ}K$. The Stokes to Stokes ratio gave a temperature of $1650^{\circ}K$. The average of the AS/S ratio data is $1643^{\circ}K$; using this procedure it appears temperature can be measured with a precision of ± 2%.

A 0.005 diameter wire Pt-Pt 10% Rh thermocouple with a bead diameter of 0.015" after coating with a protective SiO_2 overcoat, read $1486^{\circ}K$. The radiation correction for the thermocouple was determined on a burner well characterized in temperature via sodium level reversal. At a gas temperature of $1650^{\circ}K$ the radiation correction was $185^{\circ}K \pm 10^{\circ}K$, resulting in a corrected thermocouple reading of $1671^{\circ}K \pm 10^{\circ}K$. The

averaged temperature from AS/S of 1643°K and temperature from Stokes to Stokes (300°K) of 1650°K are low by about 2% indicative of the accuracy possible with the procedure employed.

Although the tunability inherent in dye lasers is highly advantageous for Raman work in regard to checking for spurious signals, it can limit temperature measurement accuracy if the laser is not precisely tuned to the proper wavelength. This is particularly true when using extremely narrow bandwidth interference filters to suppress noise detection as shown in Fig. 18. There the computed behavior of the AS/S ratio is displayed for varying bandwidth filters for three different laser line center wavelengths. The 5917Å wavelength centers the room air Raman signals at the center of the filter passbands; also shown is the effect of a 5Å shift in laser frequency. As seen, the Raman ratios are extremely laser wavelength sensitive due to the large N_2 Q-branch shifts arising from the vibrational-rotational interaction effect and the anharmonicity of the molecule. Even well calibrated grating wavelength meters may be off by a few Angstroms as the grating is tuned from a He-Ne laser alignment setting of 6328Å. It is also tedious to have to measure linecenter wavelength everytime one wishes to make a temperature measurement. In the experiments just described, the grating readout on the laser was used only as a rough guide. The grating was set by tuning the laser to maximize the room air Stokes signal. In addition, because interference filters are extremely angle sensitive, the photomultiplier tubes which housed the filters, were spring mounted, amenable to "mirror-like" adjustment. This permitted the interference filters to be aligned normal to the collected scattering obviating any shifting of the filter's center passband wavelength. This procedure apparently

works fairly well judging from the accuracy to which the temperature measurements were made. Clearly though, in low noise situations, it would be most advantageous to use the widest bandwidth filters tolerable.

Seeded Flame Measurements

Laser induced particulate noise was introduced into the experiment using the apparatus shown in Fig. 19. A 0.64 cm OD, 0.24 cm ID stainless tube was inserted along the axis of the 7.6 cm dia. premixed flat flame burner previously used for the clean flame measurements. The tube was butted against the bottom surface of the stainless steel honeycomb mesh used to stabilize the premixed flat flame. Methane or a methane/nitrogen combination was flowed through the tube to produce a diffuse diffusion flame on the centerline of the burner as seen in Fig. 19. By varying the methane and nitrogen flowrates, the laser induced particulate noise could be adjusted as desired. The spectrometer was arranged in a four channel fashion as seen in Fig. 20. The anti-Stokes and Stokes filters were at 5200 and 6864Å respectively; anti-Stokes and Stokes "noise" filters were placed at 5230 and 6811Å to sample the noise. The spectrometer was set up to detect backscattering and purposely arranged for low spatial resolution, ~ 3 cm. The idea was to introduce noise into the temperature measurement experiment, but in a manner so as not to alter the temperature field greatly. This would then permit comparison of measurements with and without the noise.

In Fig. 21, noise sampling and subtraction are displayed. The CH_4/N_2 seed flowrates were adjusted to produce an anti-Stokes S/N near unity. The Stokes S/N turned out to be higher, on the order of five. The noise photomultiplier tube voltages were adjusted to produce on average good subtraction. In Fig. 21 the noise produced on both the anti-Stokes and Stokes signal channels is shown. The laser was tuned to 5980Å so that no Raman signals were present in any of the four filter passbands. There is an interesting sidelight to the noise displayed. With a pure methane seed, laser induced particulate temperatures could be ascertained in the usual manner. With N_2 diluent, however, artificially high temperatures were obtained. Although the exact reason for this is unclear, we suspect possible laser induced interfering emissions (or absorptions) from NO_2 which has a strong thermal and recombination continuum from 5000Å to the near infrared (Ref. 37). Also shown in Fig. 21 is the subtraction between the signal and noise channels. Good subtraction required adjustment of the noise photomultiplier voltages in ten volt increments. Due to shot noise, subtraction is not perfect on any one shot as previously mentioned and one attempts to adjust the voltages so that the subtraction error fluctuates on either side of zero.

In Fig. 22, the results of the seeded "temperature" measurement are shown. After adjusting the noise tube voltages for good subtraction on average, the laser was tuned to 5917Å placing the N_2 Raman scattering within the signal tube passbands. After observing the Raman scattering with the seed on, the seed was turned off and the two signals compared. For these demonstrations, the polarization filter was

removed from the spectrometer to increase the photon level reaching the tubes, and no attempt was made to extract temperature information from the ratios in the manner previously described. As seen the ratios ("temperatures") are very close with and without the seed on. The ratio with the seed on is actually somewhat higher and the absolute signal levels somewhat lower due to the additional energy release from the diffusion flame. This was verified by thermocouple probing the flame every 2 mm which showed the central two centimeters of the burner to be about 150^{o}K hotter with the diffusion flame present.

Subtraction in lower S/N situations was not attempted since shot noise would obscure the situation photographically. As previously mentioned, leakage currents on our signal averager prevented its usage at low laser pulse rates. Nevertheless, the foregoing experiment demonstrates the feasibility of noise sampling and subtraction and practical implementation is straightforward.

CONCLUSIONS AND RECOMMENDATIONS

It is difficult to be categorical in regard to the utility of spontaneous Raman scattering for practical combustion diagnostics since conditions can vary widely from device to device and within a given device depending on location and operating parameters. Primary zone diagnostics in a diffusion flame apparatus operating on hydrocarbon fuels appears highly doubtful based on both background luminosity considerations and laser induced particulate noise effects. Secondary and exhaust region probing may be possible (Ref. 6) since luminosity levels tend to be lower, but particulate effects could be problematical if the particles are present in sufficient quantity or size. High focal flux levels appear optimal for enhancing Raman S/N in regard to laser induced particulate noise but may lead to problems with window breakdown and fluorescence. The latter may be sufficiently strong to preclude the use of preferred background luminosity suppression geometries. Noise sampling and subtraction is feasible as has been demonstrated. However, shot noise effects dictate that Raman data be separately averaged to permit accurate determination of average signal levels. Ensemble averaging, however, leads to band intensity ratios which, in fluctuating environments, depend not only on average temperature, but on average density and on the magnitude and correlations of fluctuations in density and temperature. These effects may result in large measurement errors rendering the extracted Raman data of little utility. Based on this perception of the situation, we believe spontaneous Raman scattering to be of limited utility for many practical applications. However, due to its relative simplicity

and high level of present day understanding it certainly merits first consideration in environments where the aforementioned noise effects are not overwhelming.

For most practical applications, the feasibility of stronger Raman processes such as CARS (coherent anti-Stokes Raman scattering) or near-resonant Raman scattering needs to be investigated. In particular CARS has shown great potential to date but is not without problems due to its sophistication. It is not completely clear at this point what the impact of practical device characteristics such as high turbulence and particulate levels will be on CARS generation. In particular since nonresonant susceptibility contributions are often problematical in CARS experiments, potential particulate (soot) noise effects should be examined in a controlled manner.

REFERENCES

1. Lapp, M. and C. M. Penney: Laser Raman Gas Diagnostics, Plenum Press, New York, 1974.

2. Lederman, S.: Modern Diagnostics of Combustion, AIAA Paper 76-26, 14th Aerospace Sciences Meeting, Washington, D.C., January 1976.

3. Setchell, R. E.: Time Averaged Measurements in Turbulent Flames Using Raman Spectroscopy, AIAA Paper 76-28, 14th Aerospace Sciences Meeting, Washington, D.C., January 1976.

4. Eckbreth, A. C.: Laser Raman Gas Thermometry, AIAA Paper 74-1144, AIAA/SAE 10th Propulsion Conference, San Diego, California, October 1974.

5. Eckbreth, A. C.: Laser Raman Thermometry Experiments in Simulated Combustor Environments, AIAA Paper 76-27, 14th Aerospace Sciences Meeting, Washington, D.C., January 1976.

6. Leonard, D. A.: Field Tests of a Laser Raman Measurement System for Aircraft Engine Exhaust Emissions, Technical Report AFAPL-TR-74-100, October 1974.

7. Eckbreth, A. C.: Raman Amplitude Modulation for Noise Suppression," United Technologies Research Center Report UTRC76-132, August 1976.

8. Mack, M. E.: Vortex Stabilized Flashlamps for Dye Laser Pumping, Appl. Opt. Vol. 13, pp. 46-55, January 1974.

9. Bowman, C. T. and L. S. Cohen: Influence of Aerodynamic Phenomena on Pollutant Formation in Combustion, Report EPA-650/2-75-061a, July 1975.

10. Chang, D. B., J. E. Drummond and R. B. Hall: High-Power Laser Radiation Interaction with Quartz, J. Appl. Phys., Vol. 41, pp. 4851-4855, November 1970.

11. Afanasev, Y. V. and O. N. Krokhin: Vaporization of Matter Exposed to Laser Radiation, Sov. Phys. JETP, Vol. 25, pp. 639-645, October 1967.

12. Williams, F. A.: On Vaporization of Mist by Radiation, Int. J. Heat Mass Trans., Vol. 8, pp. 575-587, 1965.

13. Leider, A. R., et al: Thermodynamic Properties of Carbon Up To the Critical Point, Carbon, Vol. 11, pp. 555-563, 1973.

14. Sleicher, C. A., Jr., and S. W. Churchill: Radiant Heating of Dispersed Particles, Ind. and Eng. Chem., Vol. 48, pp. 1819-1824, October 1956.

15. Smith, D. C.: Gas Breakdown with 10.6-μ-Wavelength CO_2 Laser Radiation, J. Appl. Phys., Vol. 41, pp. 4501-4505, October 1970.

16. Smith, D. C. and R. T. Brown: Aerosol-Induced Air Breakdown with CO_2 Laser Radiation, J. Appl. Phys., Vol. 46, pp. 1146-1154, March 1975.

17. Photomultiplier Manual, RCA Technical Series, PT-61, 1970.

18. Robben, F.: Noise in the Measurement of Light with Photomultipliers, Appl. Opt., Vol. 10, pp. 776-796, April 1971.

19. Lencioni, D. C., and H. Kleiman: Effects of Aerosol Particle Heating on Laser Beam Propagation, MIT Lincoln Laboratory Report LTP-27, July 1974.

20. Dalzell, W. H., and A. F. Sarofin: Optical Constants of Soot and Their Application to Heat Flux Calculations, ASME J. Heat. Trans., 91, pp. 100-104, February 1969.

21. Coarse Air Cleaner Test Dust, GM Phoenix Laboratory, AC Spark Plug Div., General Motors Corporation, Flint, Michigan.

22. Plass, G. N.: Mie Scattering and Absorption Cross Sections for Aluminum Oxide and Magnesium Oxide, Appl. Opt., Vol. 3, pp. 867-872, July 1964.

23. Handbook of Chemistry and Physics, Chemical Rubber Publishing Co., Cleveland, Ohio.

24. Lederman, S.: Modern Diagnostics of Combustion, AIAA Paper 76-26, 14th Aerospace Sciences Meeting, Washington, D.C., January 1976.

25. Dalzell, W. H., G. C. Williams and H. C. Hottle: A Light Scattering Method for Soot Concentration Measurements, Comb. Flame, Vol. 14, pp. 161-170, 1970.

26. Bonczyk, P. A., United Technologies Research Center, unpublished data.

27. Kunugi, M. and H. Jinno: Determination of Size and Concentration of Particles in Diffusion Flames by a Light-Scattering Technique, 11th Symposium (International) on Combustion, pp. 257-266, August 1966.

28. D'Alessio, A., et al: Soot Formation in Methane-Oxygen Flames, 15th Symposium (International) on Combustion, pp. 1427-1438, August 1974.

29. Wuerker, R. F., H. M. Goldenberg and R. V. Langmuir: Electrodynamic Containment of Charged Particles by Three-Phase Voltages, J. Appl. Phys., Vol. 30, pp. 441-442, 1959.

30. Haught, A. F. and D. H. Polk: High-Temperature Plasmas Produced by Laser Beam Irradiation of Single Solid Particles, Phys. Flds., Vol. 9, pp. 2047-2055, October 1966.

31. Zavitsanos, P. D.: Mass Spectrometric Analysis of Carbon Species Generated by Laser Evaporation, Carbon, Vol. 6, pp. 731-737, 1968.

32. Howe, J. A.: Observations on the Maser Induced Graphite Jet, J. Chem. Phys., Vol. 39, pp. 1362-1363, September 1963.

33. Jeunehomme, M. and R. P. Schwenker: Focussed Laser-Beam Experiment and the Oscillator Strength of the Swan System, J. Chem. Phys., Vol. 42, pp. 2406-2408, April 1965.

34. Mentall, J. E. and R. W. Nicholls: Spectroscopic Temperature Measurements on Laser-Produced Flames, J. Chem. Phys., Vol. 46, pp. 2881-2885, April 1967.

35. Vasil'yev, YE. P., YE. A. Yefremova and M. V. Stradomskiy: Investigation of Certain Spectral Characteristics of Flames on Combustion of Liquid Fuel, Heat Transfer - Soviet Research, Vol. 7, pp. 108-111, Jan-Feb 1975.

36. Davenport, W. B. and W. L. Root, Random Signals and Noise, McGraw-Hill, New York, 1958.

37. Levitt, B. P.: Temperature and Wavelength Dependence of the Thermal Emission and O-NO Recombination Spectra of NO_2, J. Chem. Phys., Vol. 42, pp. 1038-1047, February 1965.

FIG. 1

SCHEMATIC OF TWO CHANNEL RAMAN SPECTROMETER

MODEL COMBUSTOR

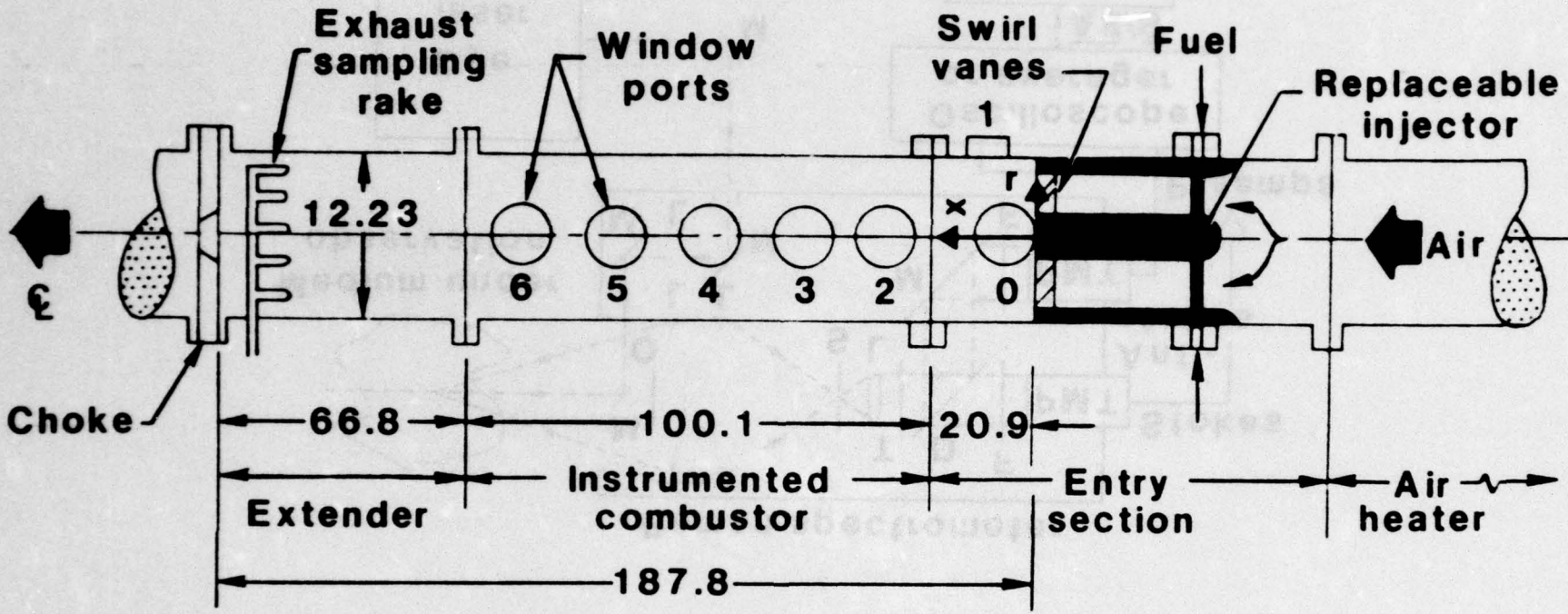

R76-952296-2

FIG 2

PARTICULATE "NOISE" IN JBTS COMBUSTOR

(MULTIPLE TRACE OVERLAYS)

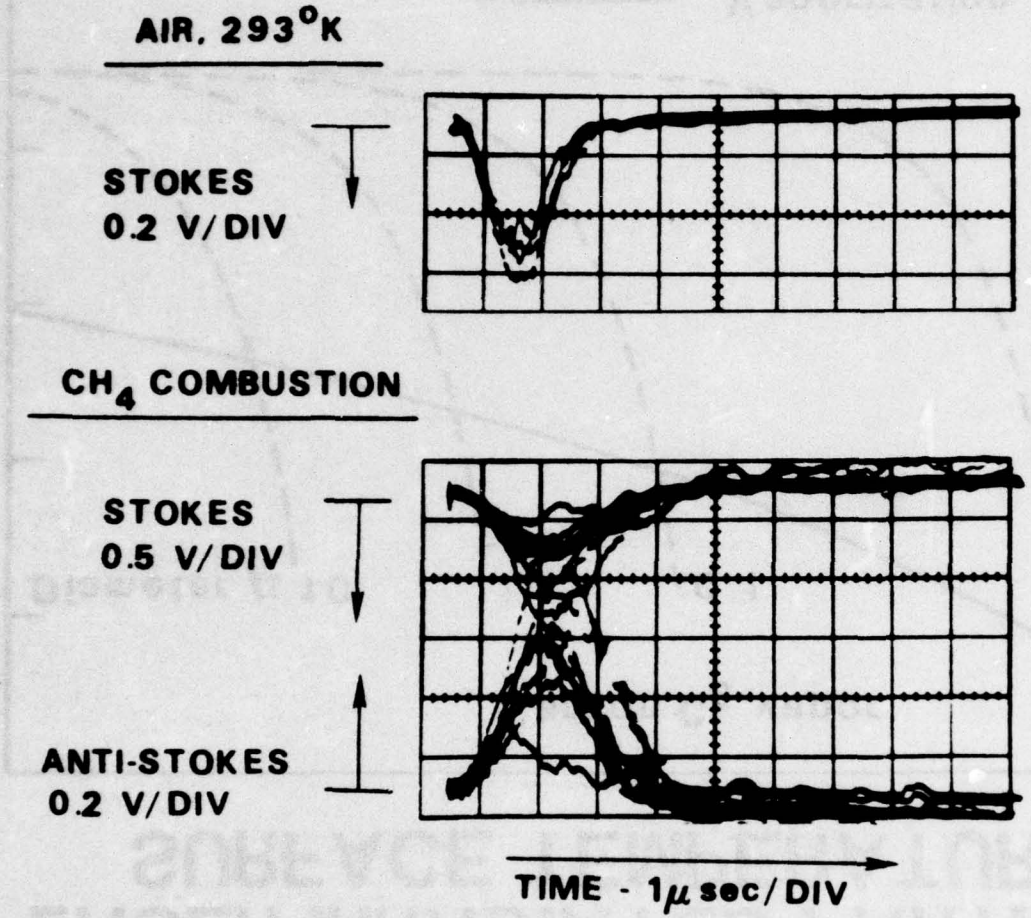

R76-952296-2

FIG. 3

LASER IRRADIATED PARTICLE SURFACE TEMPERATURE

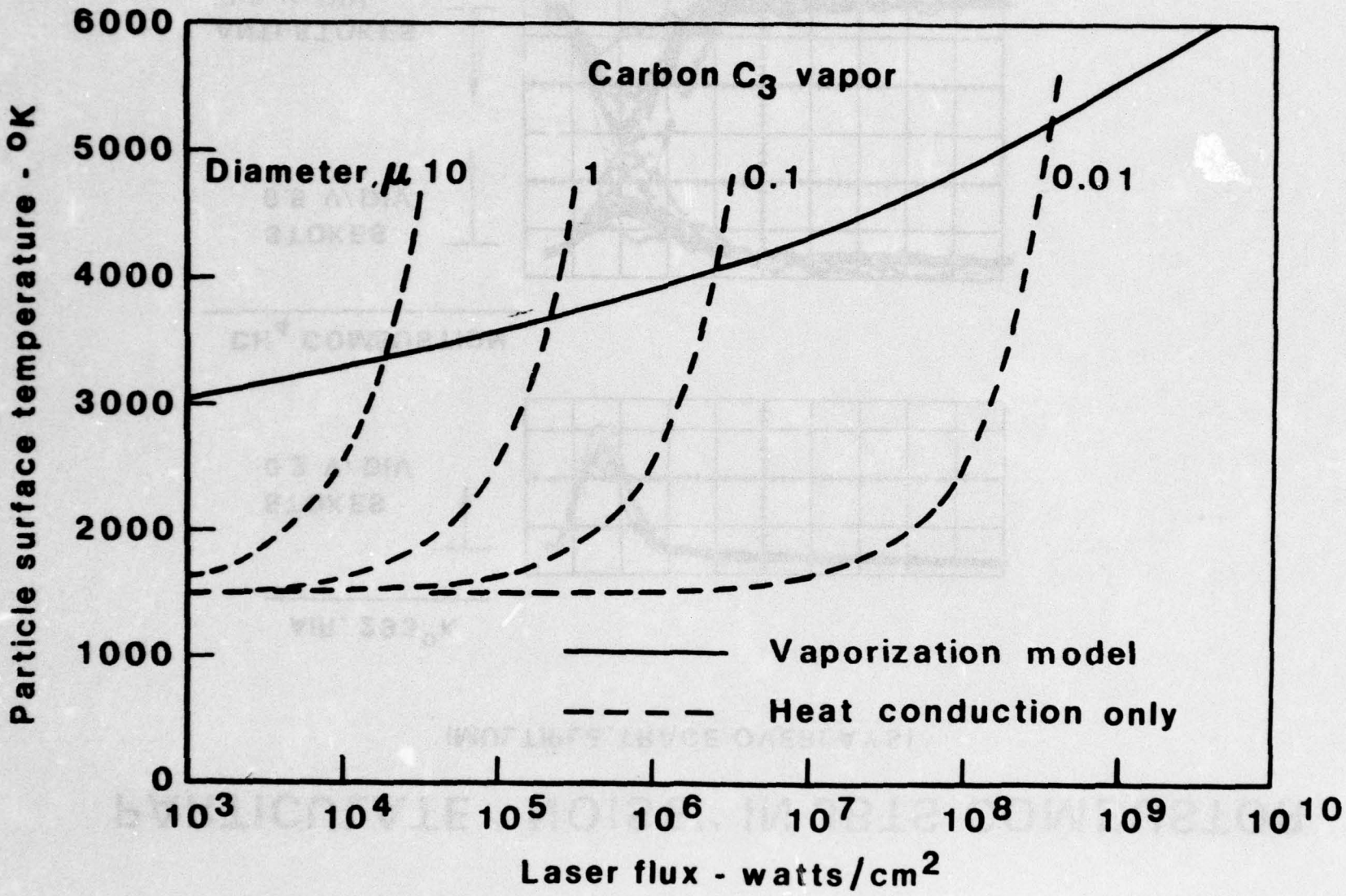

R76-952296-2

FIG. 4

TWO CHANNEL SUBTRACTION ACCURACY

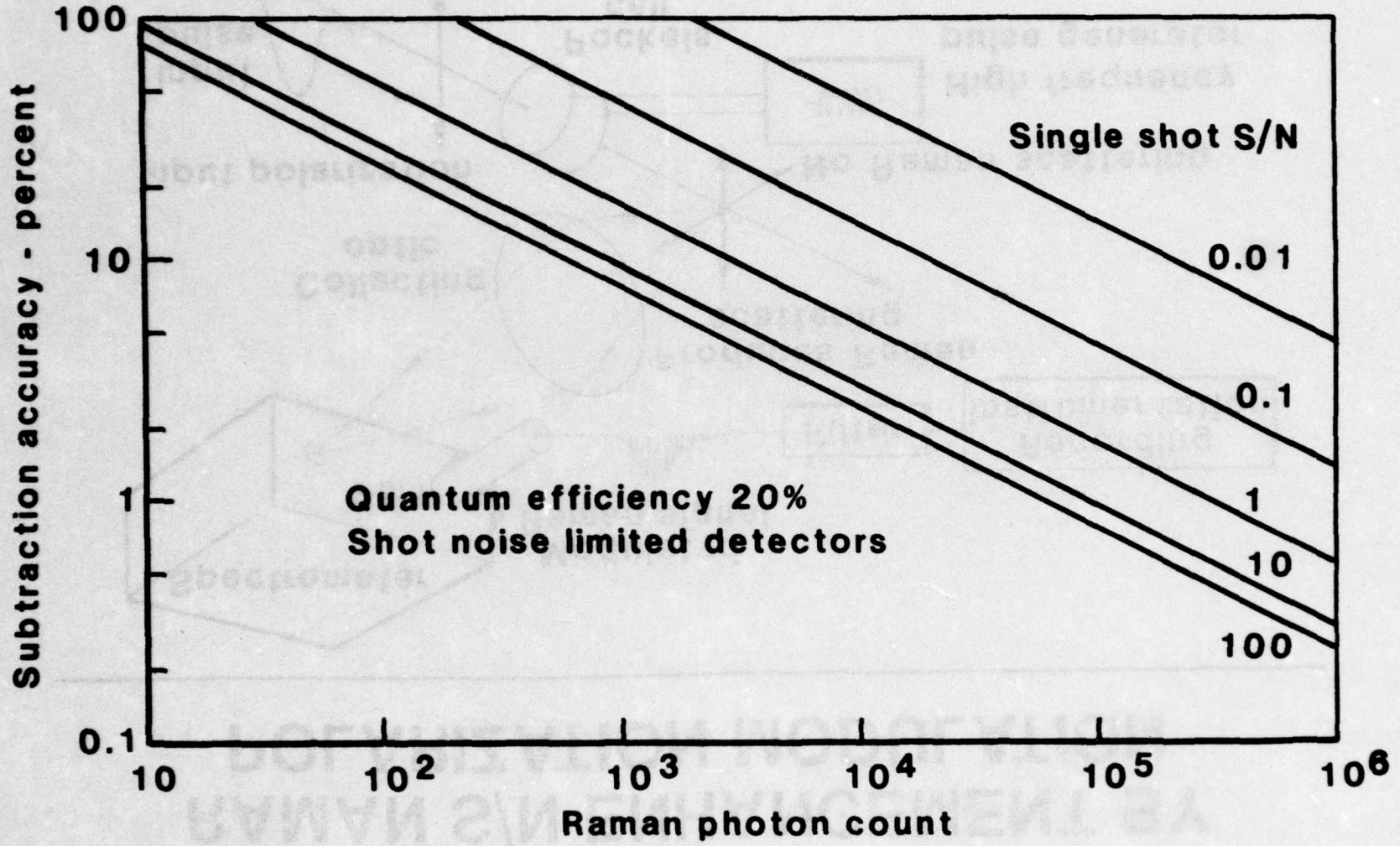

R76-952296-2

FIG. 5

R12-175-

RAMAN S/N ENHANCEMENT BY POLARIZATION MODULATION

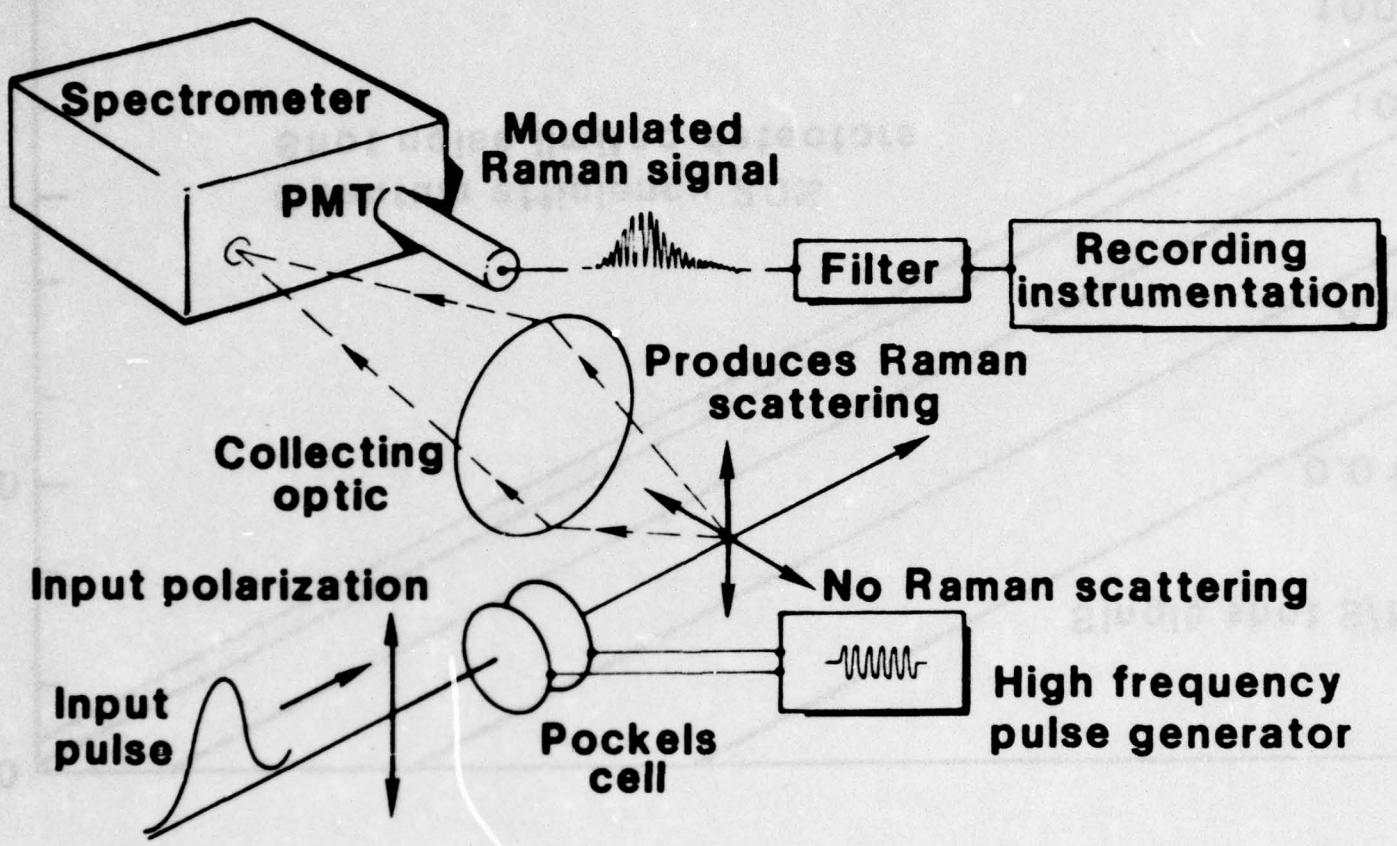

R76-952296-2

FIG. 6

FIG. 7

LASER IRRADIATED PARTICLE HEATING EXPERIMENT

LASER IRRADIATED GRAPHITE EMISSION

Dye laser wavelength 5950 Å

C_2 Swan system

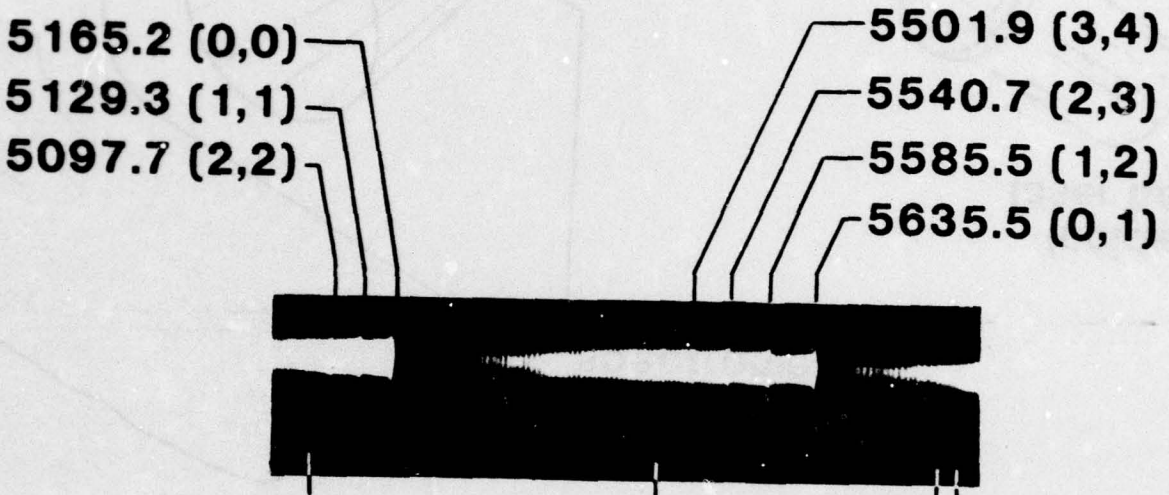

R76-952296-2

76-04-173-3

FIG. 8

Laser Induced Particulate Noise Apparatus

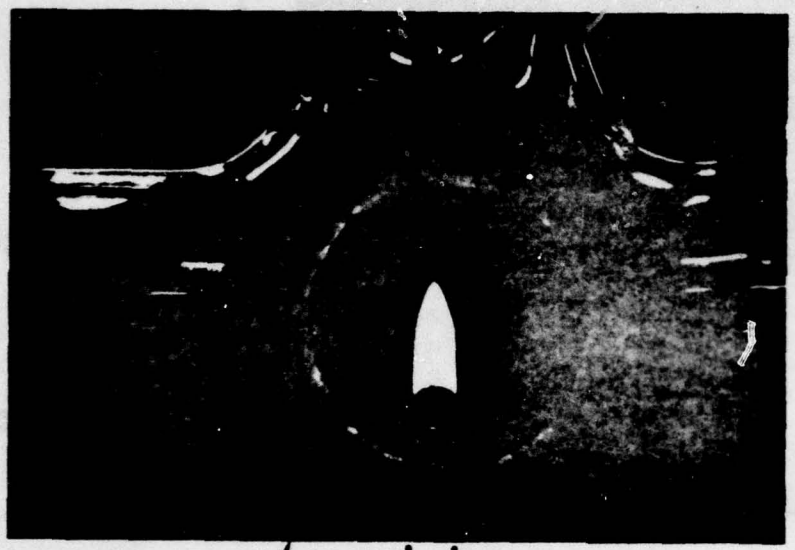

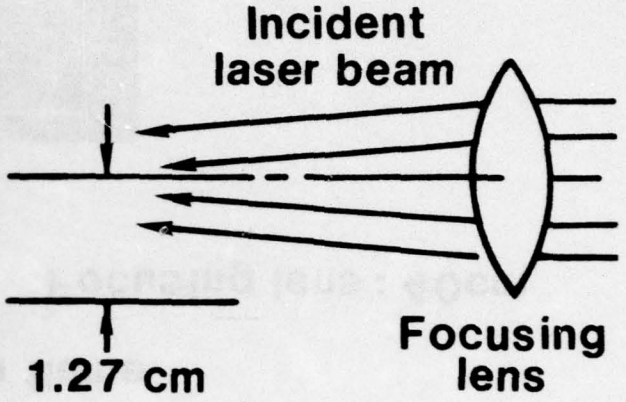

Viewing port

0.64 cm

C_3H_8, 0.6 gm/sec

R76-952296-2

FIG. 9

R76-952296-2

Laser Induced Particulate Noise

Triple trace overlay

Laminar propane diffusion flame

Pulse energy: 260mJ **Focusing lens: 40cm**

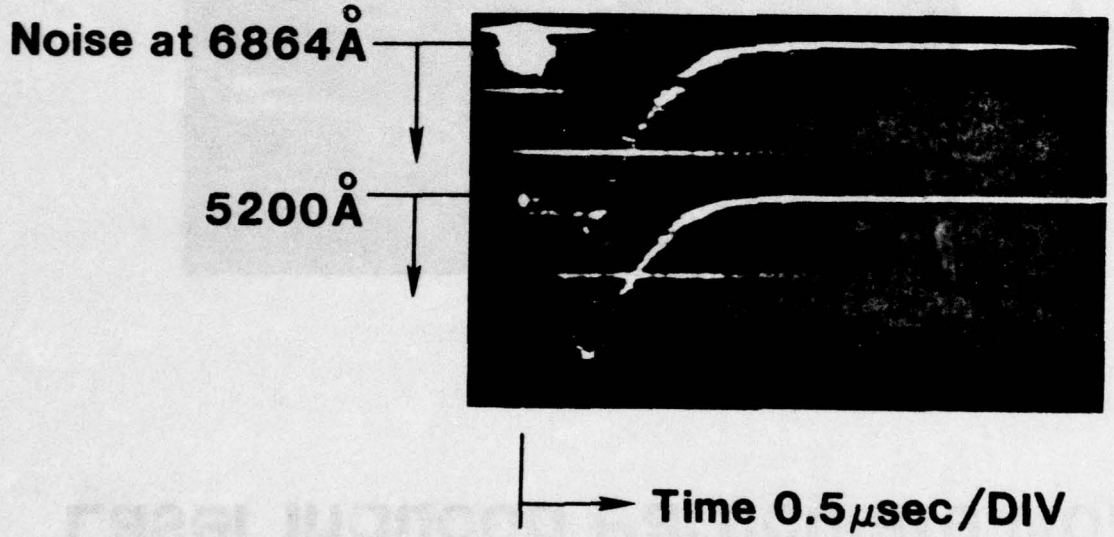

76-08-7-1

FIG. 10

Laser Irradiated Particle Surface Temperature

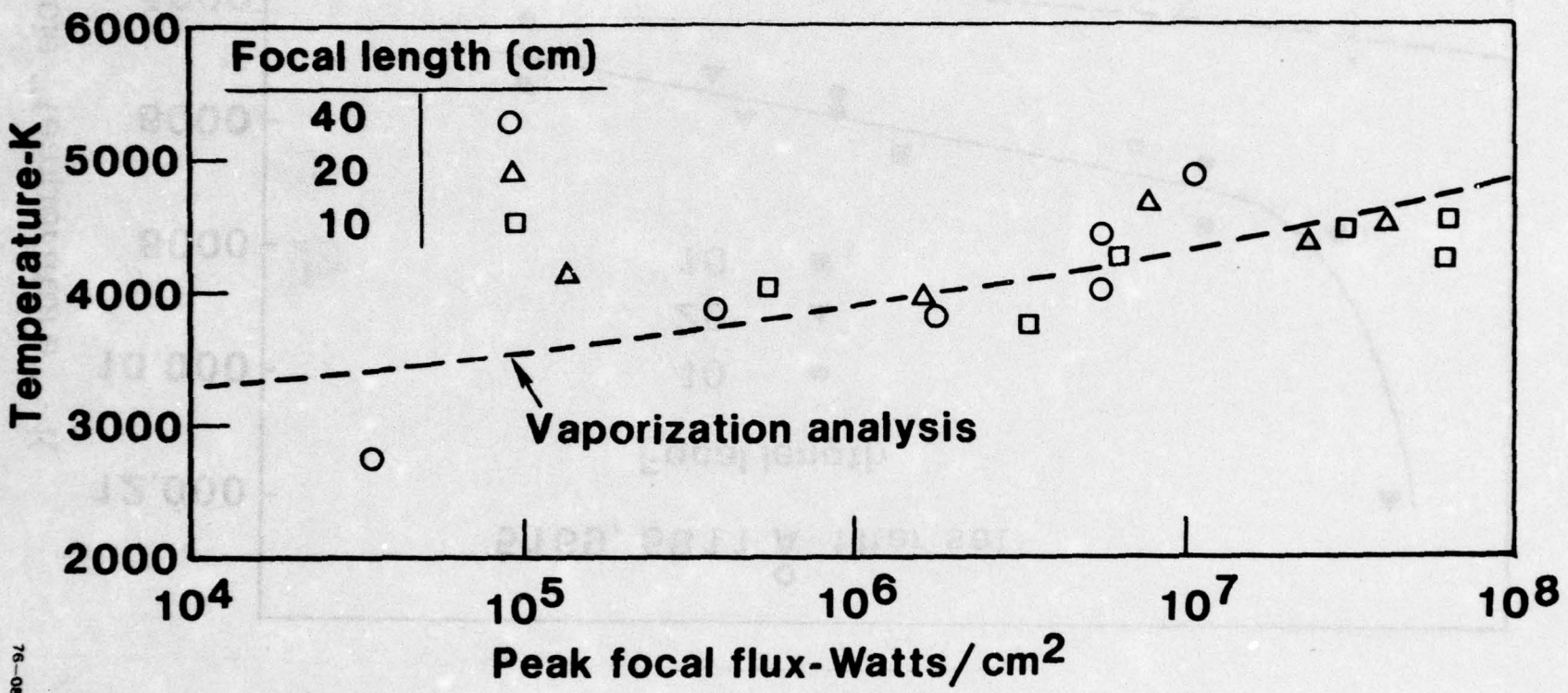

76-08-7-4

FIG. 11

Particle "Temperature" with Alternate Filter Set

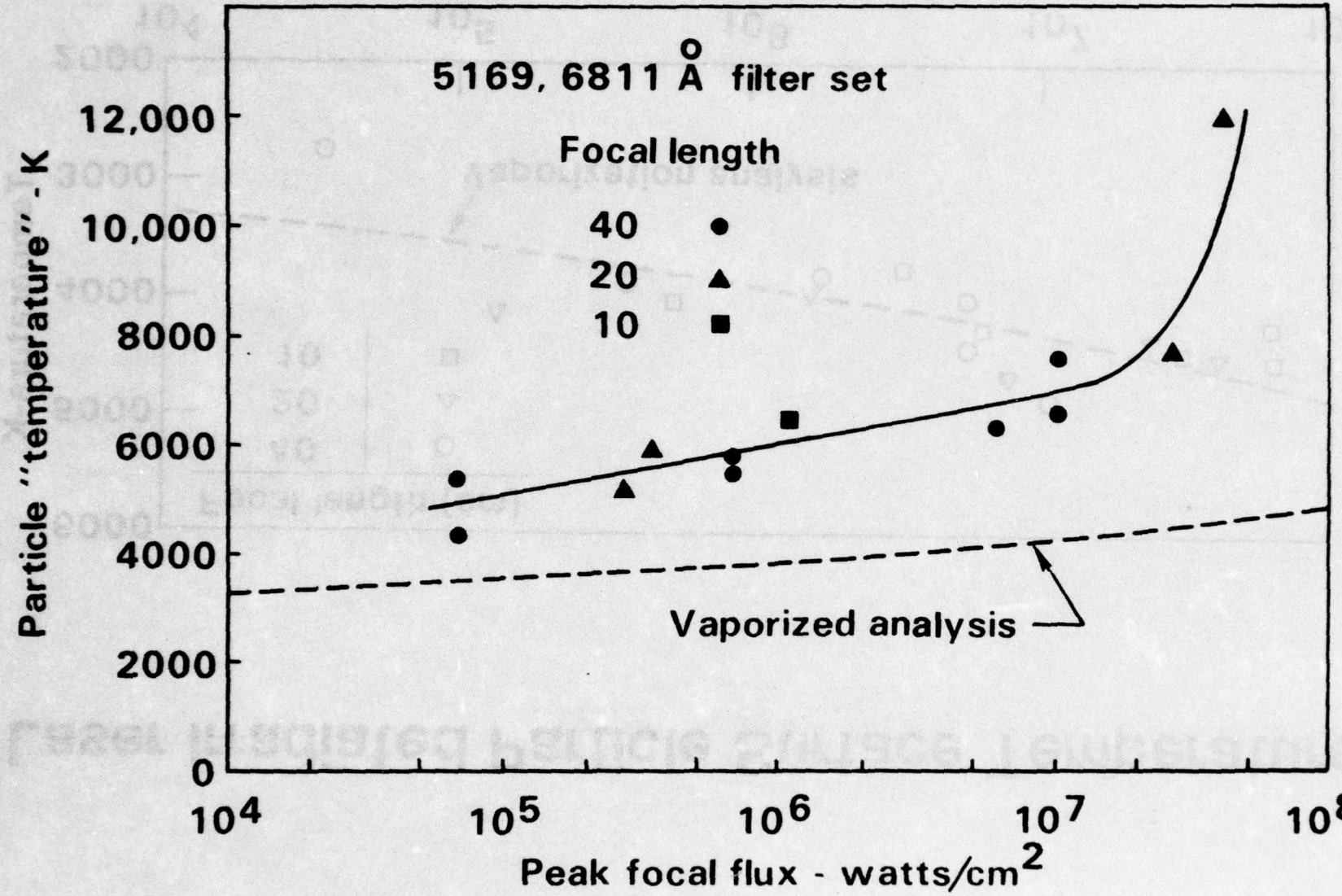

R76-952296-2

FIG. 12

76-08-7-3

Laser Induced Particulate Noise Scaling

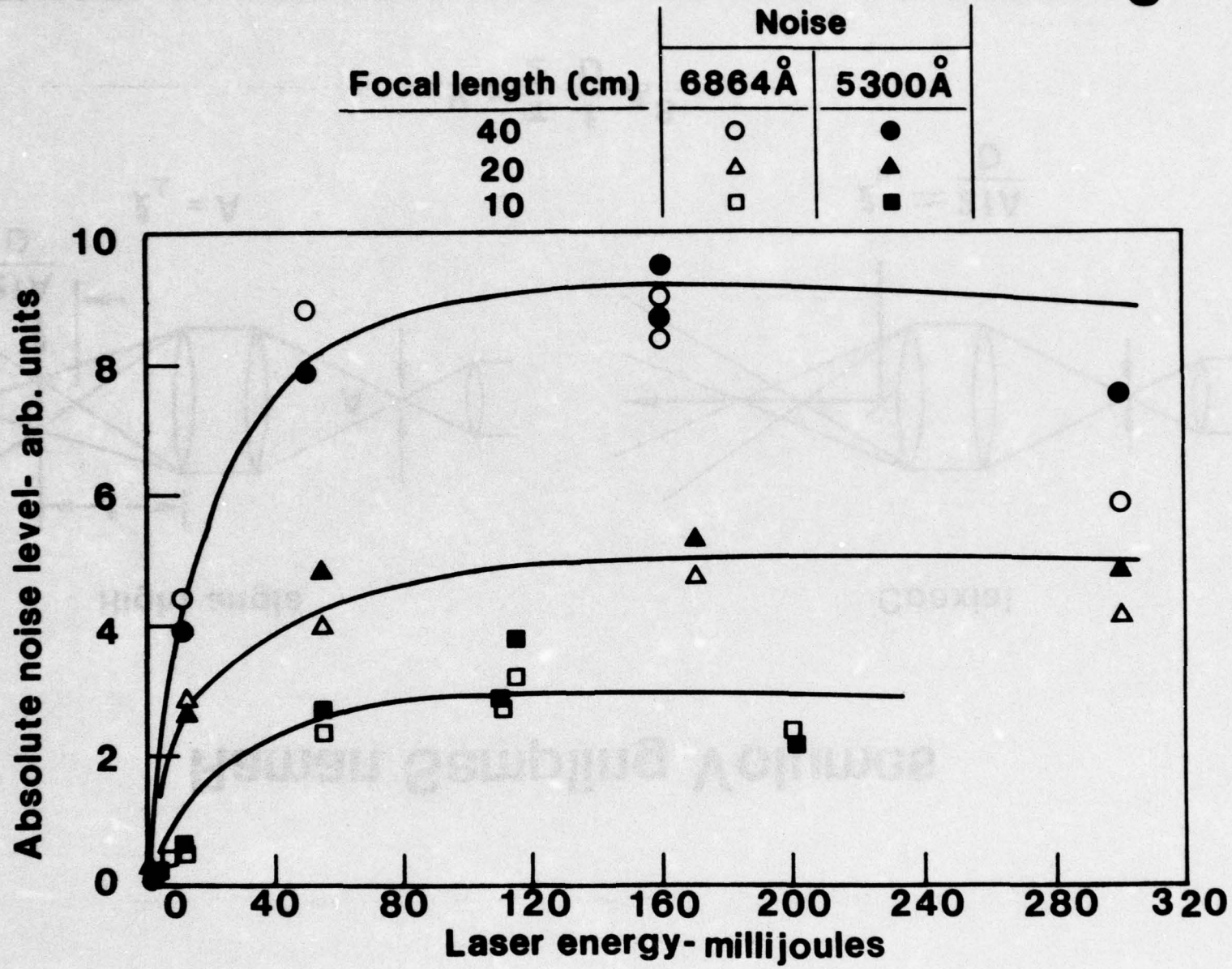

R76-952296-2

FIG. 13

76-08-7-2

R76-952296-2

Raman Sampling Volumes

Right angle

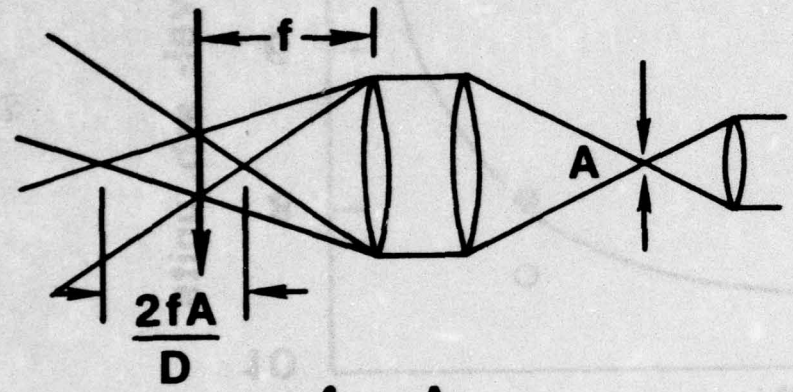

$$\ell_{\perp} = A$$

Coaxial

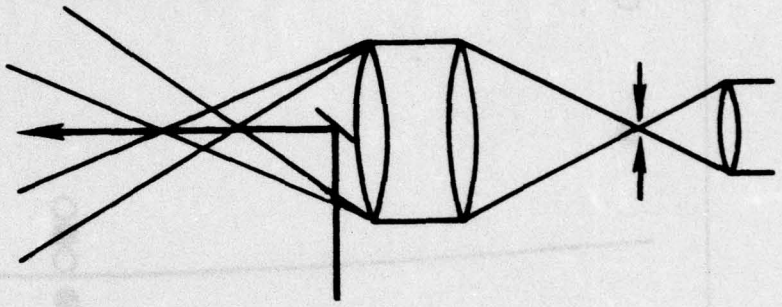

$$\ell_{\parallel} \simeq \frac{2fA}{D}$$

$$V = \frac{\pi}{2} \frac{f}{D} A^3$$

76-06-117-1

FIG. 14

Bandwidth Factor Variation with N_2 Temperature

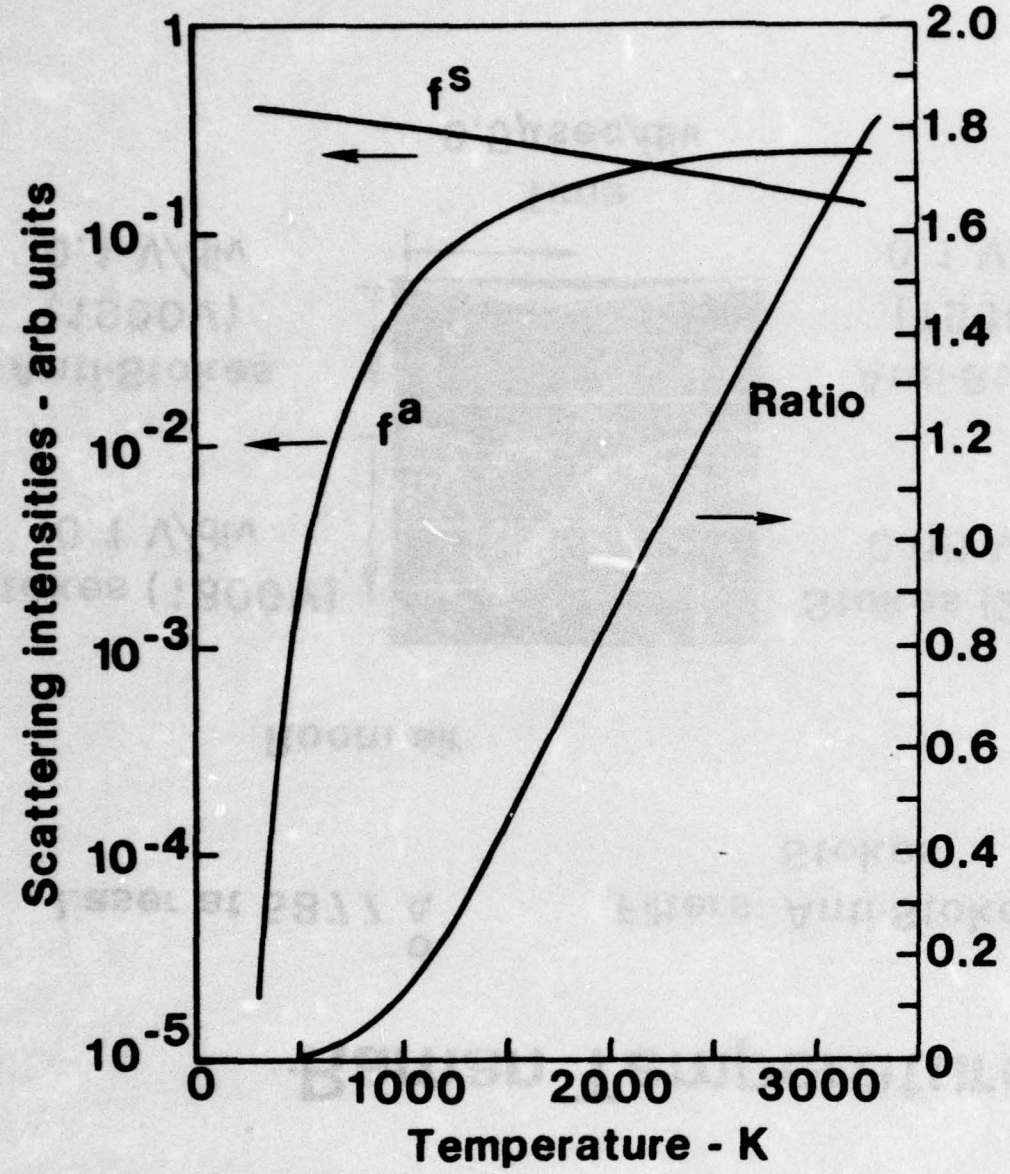

Laser (Lorentzian)
5917 Å, 6Å FWHH

Filters (Gaussian)
Stokes:
6864Å, 12Å FWHH
Anti-Stokes:
5200, 11

R76-952296-2

FIG. 15

76-08-92-1

Raman Temperature Data

Laser at 5877 Å

Filters: Anti-Stokes 5169, 10.5 A FWHH
Stokes 6811.5, 11.5

Room air

Stokes (1800V)
0.1 V/div

Anti-Stokes
(1900V)
0.1 V/div

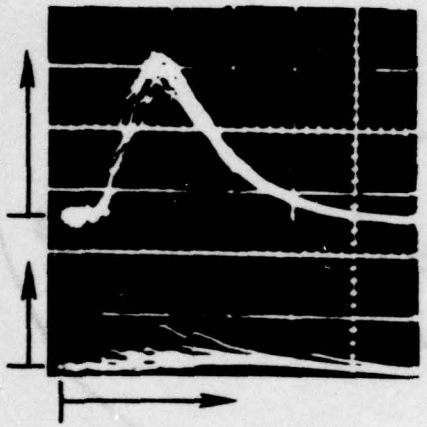

Time
0.5μsec/div

Flame

Stokes (2000V)
0.05 V/div

Anti-Stokes
(1900V)
0.1 V/div

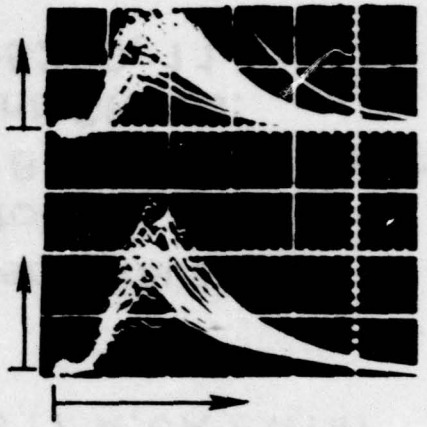

Time
0.5μsec/div

R76-952296-2

72

76-08 214-3

FIG. 16

Raman Ratio Variation with Temperature

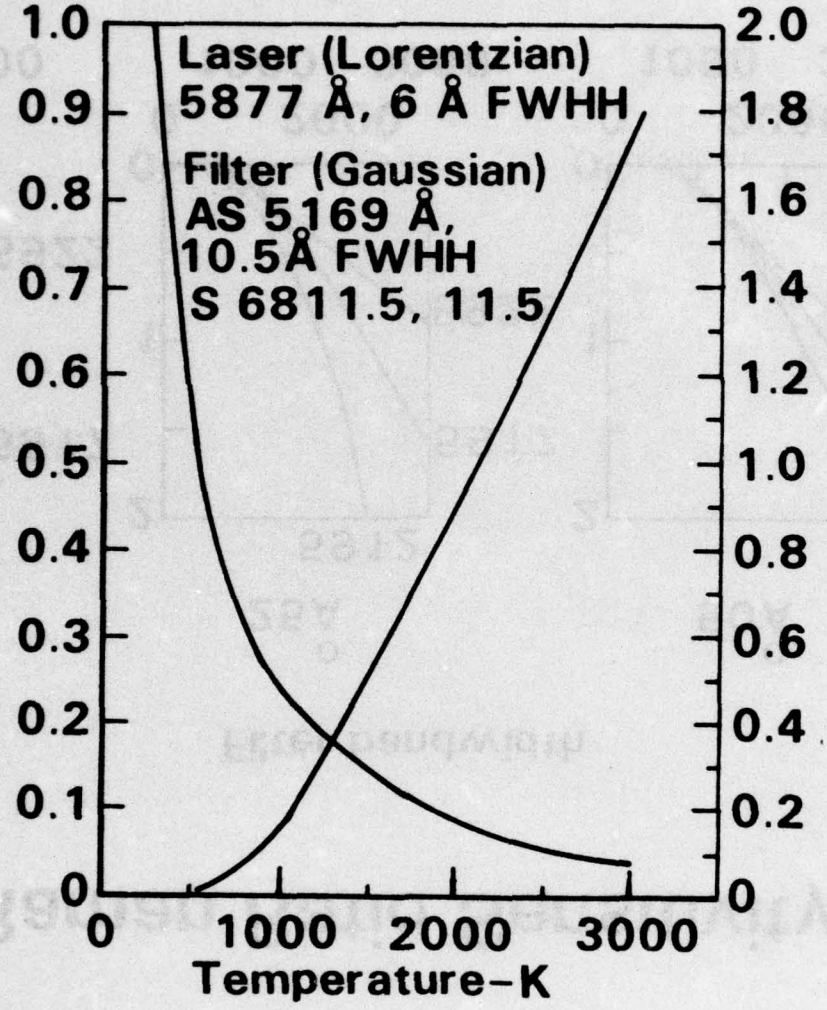

Stokes (T) to Stokes (300°K) ratio

Anti-Stokes to Stokes ratio

76-08-201-1

R76-952296-2

FIG. 17

FIG. 18

Raman Ratio Sensitivity

76-08-214-2

Compound Diffusion/Premixed Flame Apparatus

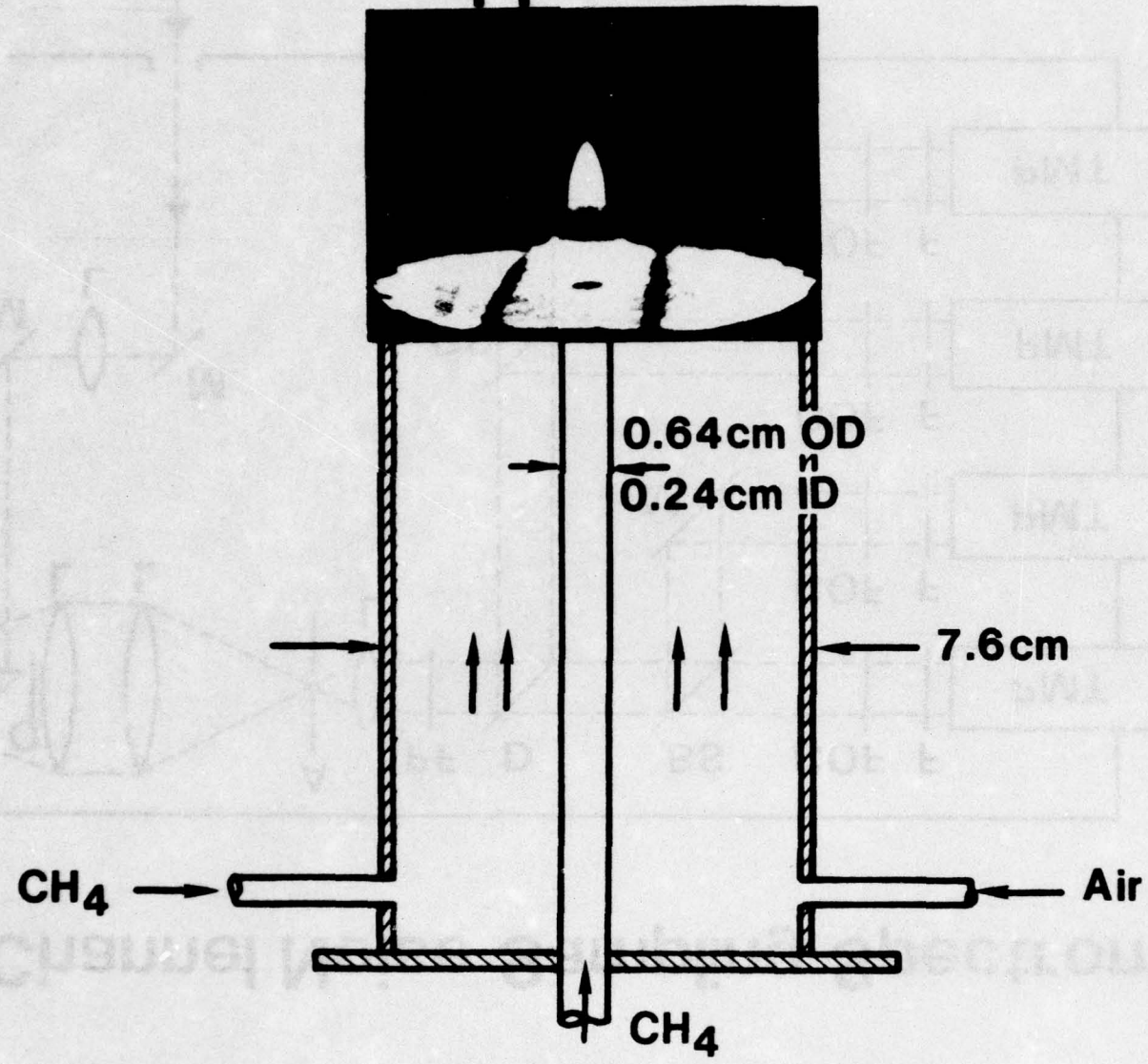

R76-952296-2

FIG. 19

FIG. 20

Four Channel Noise Sampling Spectrometer

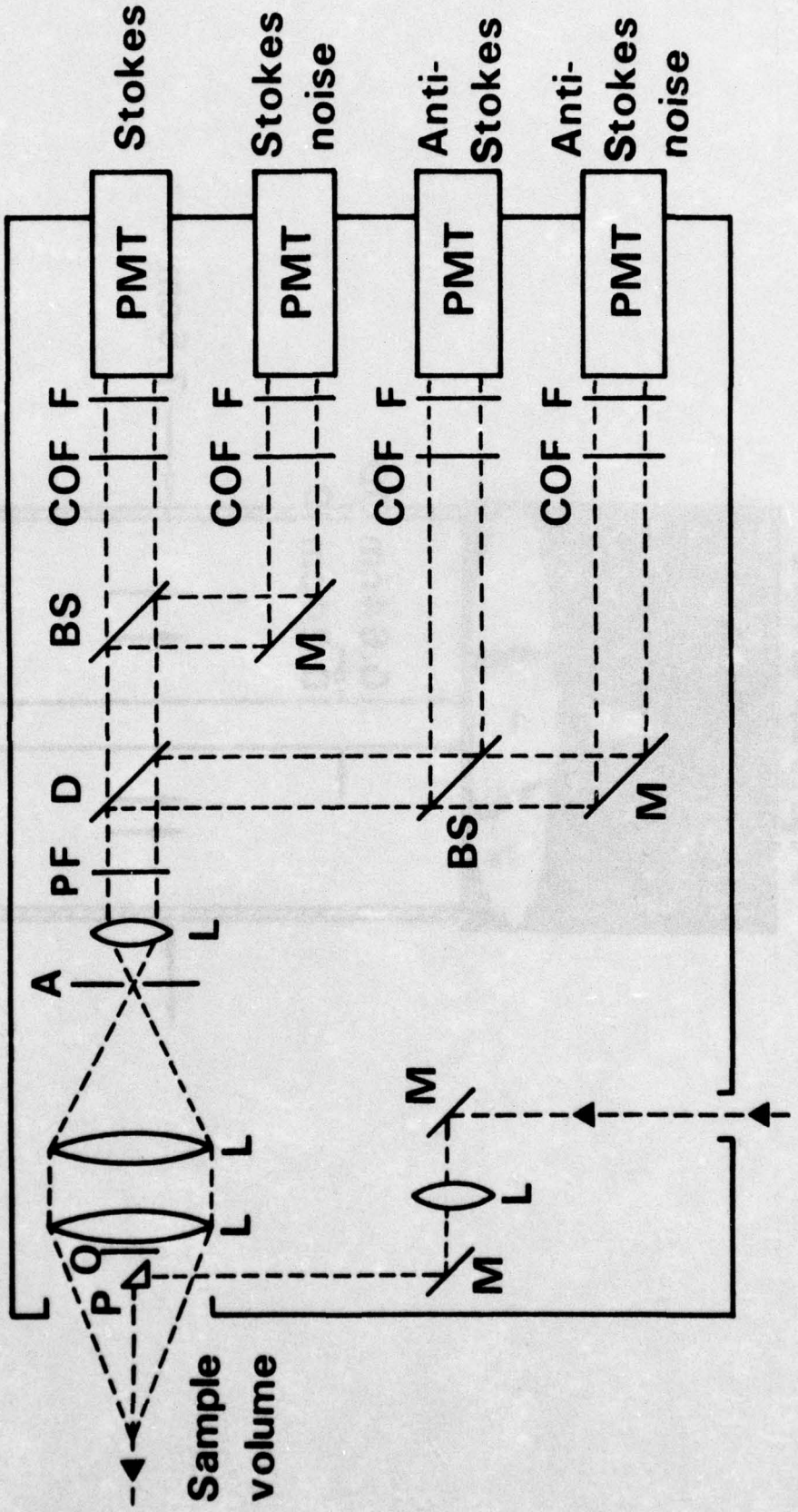

76-08-214-1

Noise Sampling and Subtraction

Laser at 5980 Å

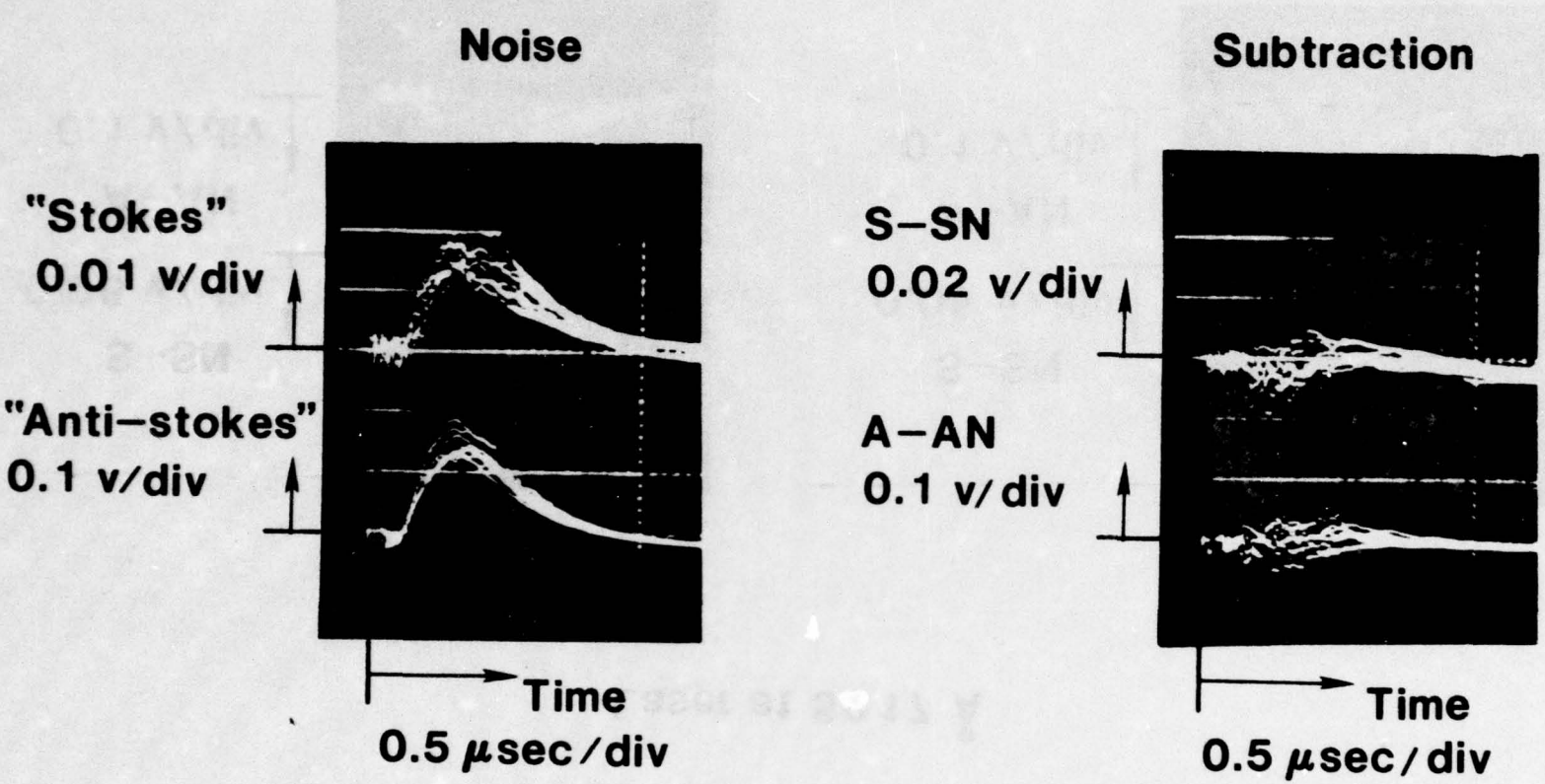

R76-952296-2

FIG. 21

"Temperature" Measurement in Seeded Flame

Laser at 5917 Å

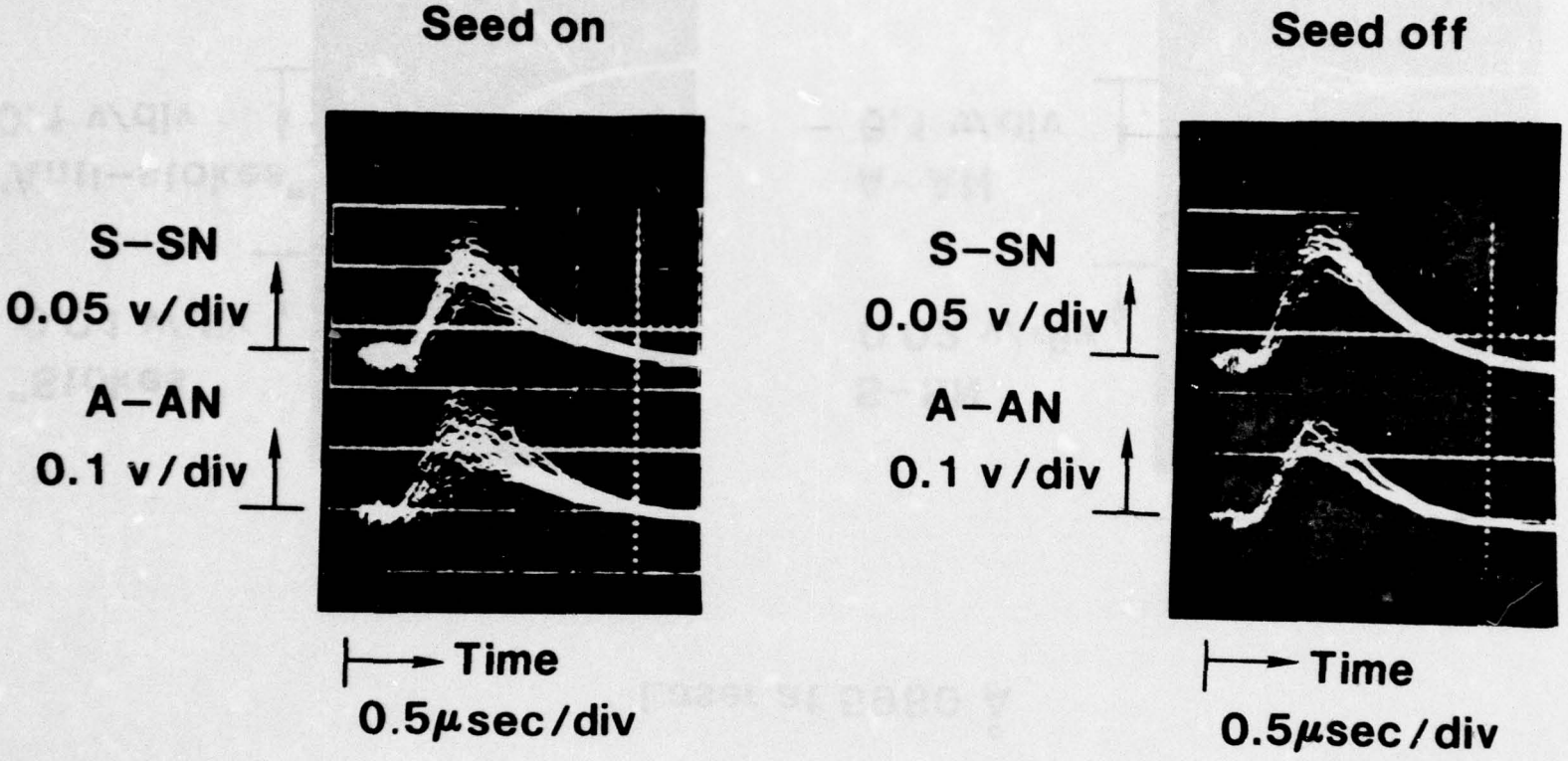

FIG. 22

APPENDIX I

LASER RAMAN THERMOMETRY

Raman Scattering

Raman scattering is the phenomenon of inelastic collision processes between photons of light and molecules be they in the solid, liquid or gaseous phase. The effect was theoretically predicted by Smekal in 1923, but was subsequently named in honor of its experimental discoverer. Raman scattering has been physically understood for some time (Refs. I-1, 2) and, with the advent of lasers, has come into wide use and application (Refs. I-3, 4).

When photons of light collide with molecules, the photons may either lose energy to or gain energy from the target molecules as seen in Fig. A-1. In the former event, termed Stokes scattering, the molecule becomes excited, and, in the latter termed anti-Stokes, the molecule is deexcited providing, of course, that it was excited prior to the collision. The energy exchanges which occur are quantized in accordance with the allowable energy levels of the molecule. The scattering processes may be expressed symbolically as follows:

Stokes

$$h\nu + N(m) \rightarrow h\nu' + N(n) \qquad \text{(I-1)}$$

$$h(\nu - \nu') = E(n) - E(m) \qquad \text{(I-2)}$$

Anti-Stokes

$$h\nu + N(n) \rightarrow h\nu'' + N(m) \qquad \text{(I-3)}$$

$$h(\nu'' - \nu) = E(n) - E(m) \qquad \text{(I-4)}$$

where h is Planck's constant; ν, the frequency of the incident photons; ν', ν'', the frequencies of the Stokes and anti-Stokes scattered photons; E(n), E(m) the energies

of the quantum states n and m, where n is assumed the more energetic of the two states. Since each molecular species possesses a characteristic set of energy states, the spectral distribution of Raman scattering will be uniquely determined by the incident laser wavelength and the species from which scattering occurs. This is the principle underlying the use of the Raman technique for species identification. When n and m represent different rotational states within a given vibrational energy level, the scattering is termed, naturally, rotational Raman scattering. When a change of molecular vibrational energy occurs, vibrational Raman scattering occurs often accompanied by a change in rotational energy as well. When no energy exchange occurs, the scattering process is elastic and is termed Rayleigh scattering. Examples of all of these processes can be seen in Fig. I-1 which displays the possible scattering processes for a diatomic molecule.

Raman Thermometry

To make temperature measurements, use is made of the fact that the intensity of scattering scales directly with the number of molecules in the initial scattering state and directly with the fourth power of the scattered frequency, thusly

$$I_S(\nu') \sim \nu'^4 N(m) \qquad \text{(I-5)}$$

$$I_A(\nu'') \sim \nu''^4 N(n) \qquad \text{(I-6)}$$

where I_S, I_A are the Stokes and anti-Stokes scattered intensities respectively. Under conditions of thermal equilibrium, the populations in the various quantum states are distributed in a Boltzmann fashion, namely,

$$\frac{N(n)}{N(m)} = e^{-[E(n)-E(m)]/kT} \qquad \text{(I-7)}$$

where k is Boltzmann's constant and T the temperature. Since the energy levels of most molecules are well known, the frequencies ν' and ν'' are accurately calculable and temperature can be obtained from a measurement of the anti-Stokes to Stokes intensity ratio

$$T = \frac{E(n) - E(m)}{k \ \ell n \ I_A(\nu'')/I_S(\nu') + 4k \ \ell n \ \nu'/\nu''} \qquad \text{(I-8)}$$

Of special note is the absence of any pressure or density dependent terms in the above expression, so that fluctuations in these parameters do not directly affect the measurement of temperature. The temperature and density indirectly affect the measurement, however, since the accuracy to which I_A and I_S can be measured depends on their absolute magnitude and, hence, from equations (I-5) and (I-6) on the magnitude of these two parameters. Also, of note, is the fact that the static or translational temperature is measured and not the stagnation temperature typically measured by physical probes, e.g., thermocouples.

The foregoing analysis for simplification merely treats two individual energy states. In actuality one typically observed scattering contributions from a vast aggregate of molecular energy states. In Appendix II, a computer code is described which treats the more complicated situation that generally pertains experimentally.

References - Appendix I

I-1 S. Bhagavantam, Scattering of Light and the Raman Effect, Chemical Publishing Co., Brooklyn, NY, 1942.

I-2 H. A. Szymanski, Raman Spectroscopy, Plenum Press, NY, 1967.

I-3 M. C. Tobin, Laser Raman Spectroscopy, Wiley-Interscience, NY, 1971.

I-4 J. Loader, Basic Laser Raman Spectroscopy, Heyden and Son, Ltd., London, 1970.

FIG. I-1

Raman Scattering Processes
V+1
V
J
3
2
1
0
Rayleigh
Q
O
S
Stokes
Anti-Stokes
Rotational
Q S O
Vibrational Stokes
Q O S
Vibrational anti-Stokes
76-08-189-1

APPENDIX II

COMPUTER CODE FOR N_2 RAMAN SCATTERING

Summary of Code

The analysis focusses on vibrational Raman scattering from N_2 which is generally the major constituent in most combustor and gas turbine situations. With vibrational Raman scattering, the Raman intensities are well displaced spectrally from the exciting line permitting the use of narrowband interference filters. In N_2, all Raman transitions as illustrated in Figure I-1 satisfying the selection rules $\Delta v = \pm 1$, $\Delta J = 0 \pm 2$ are possible. The $\Delta J = 0$ transitions are termed the Q branch, the $\Delta J = \pm 2$ are termed the S and O branches respectively for Stokes scattering and vice-versa for anti-Stokes. The analysis considers all possible transitions appropriately weighting each by the population in each initial state, line strength factors, scattered wavelength, filter bandpass, etc. The analysis is capable of treating the broadband emissions typical of dye laser sources. The analysis provides as output the relative intensities of the fundamental Stokes Q-branch, total Stokes and anti-Stokes intensities, and AS/S ratio as the function of temperature. Since the absolute intensity of the fundamental Stokes Q-branch is calculable, absolute values of intensities can be obtained for the total Stokes and anti-Stokes signals.

Wavelength of Scattering

For a diatomic molecule such as N_2, the internal energy of the molecule in vibrational state v and rotational state J can be expressed analytically (Ref. II-1) as

$$\frac{E(v,J)}{hc} = \omega_e(v+\tfrac{1}{2}) - \omega_e\chi_e(v+\tfrac{1}{2})^2 + \omega_e y_e(v+\tfrac{1}{2})^3 + B_o J(J+1) - \alpha_e vJ(J+1) \qquad \text{(II-1)}$$

where c is the speed of light and ω_e, $\omega_e\chi_e$, $\omega_e y_e$, α_e and B_o are fundamental constants of the molecule. For N_2, these quantities have the following values (Ref. II-1), in units of cm^{-1}:

ω_e	$\omega_e\chi_e$	$\omega_e y_e$	B_o	α_e
2359.61	14.456	0.00751	2.001	0.0187

For Raman scattering from an initial state v, J to a final state v', J', the energy exchange which occurs with the incident photon may be expressed as

$$\Delta E^{v,J}_{v',J'}/hc = \omega_e(v-v') + \omega_e\chi_e(v'-v)(v'+v+1) - B_o(J'-J)(J'+J+1) - \alpha_e[vJ(J+1)-v'J'(J'+1)] \qquad \text{(II-2)}$$

subject to the selection rules

$$v'-v = \pm 1,\ J'-J = \pm 2,\ 0 \qquad \text{(II-3)}$$

From energy conservation, the wavelengths of the scattered light can be calculated,

$$E' = E \pm \Delta E^{v,J}_{v',J'} \qquad \text{(II-4)}$$

where E is the photon energy, $\frac{hc}{\lambda}$, and primes denote the scattered light. Defining $\Delta\lambda = \lambda'-\lambda$ where $\Delta\lambda$ may be positive or negative, it can be shown

$$\lambda' = \lambda\left(1 - \frac{\pm\Delta E^{v,J}_{v',J'}}{E \pm \Delta E^{v,J}_{v',J'}}\right) \qquad \text{(II-5)}$$

Scattered Intensity

The intensity of scattering events into λ' may be written as (Ref. II-1)

$$S^{v,J}_{v',J'} \sim \frac{n(v,J)}{h\lambda'^4} \left(a_o \delta^J_{J'} + b^J_{J'}\right) d^v_{v'} \qquad \text{(II-6)}$$

where $n(v,J)$ is the population of the initial state (v,J) and λ'^4 reflects the scaling of the differential cross section with the scattered wavelength. $d^v_{v'}$ reflects the scaling by the square of the dipole matrix elements for the vibrational Raman transition from the initial state v and is given by (Ref. II-2)

$$d^v_{v'} = \begin{array}{ll} v+1 & \text{for } v < v' \\ v & \text{for } v > v' \end{array} \qquad \text{(II-7)}$$

The terms $b^J_{J'}$ are the rotational counterpart of the above (i.e., the scaling of the square of the matrix elements with J) and are termed the Placzek-Teller coefficients and are as follows (Ref. II-3)

$$b^J_{J'} = \begin{cases} \dfrac{J(J+1)}{(2J-1)(2J+3)} & J'-J = 0 \\ \dfrac{3(J+1)(J+2)}{2(2J+1)(2J+3)} & J'-J = 2 \\ \dfrac{3J(J-1)}{2(2J+1)(2J-1)} & J'-J = -2 \end{cases} \qquad \text{(II-8)}$$

a_o is the so-called trace scattering constant (Ref. II-1) and can be shown to be

$$a_o = \frac{3-4\rho_P}{f\rho_P} \qquad \text{(II-9)}$$

where ρ_P is the depolarization ratio and f an integer dependent on the polarization states of the laser and detecting apparatus. f is summarized in Table II-1

Table II-1

f values

	detector analysis	
laser input	polarized	unpolarized
polarized	4	7
unpolarized	7	13

Population Distribution

The population in state v, J may be written as

$$n(v,J) = n(v)F_J \tag{II-10}$$

where $n(v)$ is the total population of the vth quantum state and F_J is that fraction of the v state with quantum number J. F_J can be expressed as

$$F_J = \frac{g_I(2J+1)e^{-hcB_oJ(J+1)/kT}}{Q_{rot}} \tag{II-11}$$

where g_I is the nuclear spin degeneracy which, for N_2, equals 6 for even J values and 3 for odd J values. Q_{rot} is the rotational partition function

$$Q_{rot} = \sum_J g_I(2J+1)e^{-hcB_oJ(J+1)/kT} \approx \frac{(2I+1)^2kT}{2hcB_o} \tag{II-12}$$

where I is the nuclear spin, equal to 1 for the ground state of N_2. The total population of the vth vibrational level is

$$n(v) = \frac{n}{Q_{vib}} e^{-E(v,0)/kT} \tag{II-13}$$

where Q_{vib} is the vibrational partition function given by

$$Q_{vib} = \sum_{v} e^{-E(v,0)/kT} \qquad \text{(II-14)}$$

For purposes of evaluating Q_{vib}, the molecule can be assumed to be harmonic with little loss of accuracy. This leads to an analytic expression for Q_{vib}, namely

$$Q_{vib} = \frac{e^{-E(0,0)/kT}}{1 - e^{-[E(1,0)-E(0,0)]/kT}} \qquad \text{(II-15)}$$

Combining Equations II-10 through II-15 permits II-16 to be reexpressed in the form

$$S^{v,J}_{v',J'} \sim \frac{g_I(2J+1)}{\lambda'^4 Q_{rot} Q_{vib}} e^{-E(v,J)/kT} d^{v}_{v'} (a_o \delta^{J}_{J'} + b^{J}_{J'}) \qquad \text{(II-16)}$$

Laser Bandwidth

To this point, it has been tacitly assumed that the exciting "line" is infinitesimally narrow. In actuality dye lasers exhibit a broad bandwidth, 50-100Å; in the experiments described here, a low finesse multilayer dielectric etalon or a grating were used to spectrally condense the dye laser emission and to tune the laser to some desired line center wavelength. The grating produced a nearly-Lorentzian shaped line with full spectral width of about 6Å at half height. In the analysis, the laser line is subdivided mathematically into a number of thin spectral segments of width, $\Delta\lambda$, and Equation (II-5) evaluated separately for each segment. The contribution from each segment is then summed, appropriately weighted by the line shape factor, $g(\lambda)$. For the total relative anti-Stokes and Stokes intensities, the contribution from each segment is further weighed by the transmission of the narrowband interference filters at the specified scattered wavelength interval, hence,

$$S_{v'J'}^{v,J} \sim \frac{g_I(2J+1)}{Q_{rot}Q_{vib}} e^{-E(v,J)/kT} d_{v'}^{v}(a_o\delta_{J'}^{J} + b_{J'}^{J}) \sum_{\lambda_o-\delta}^{\lambda_o+\delta} \frac{g(\lambda)f(\lambda')\Delta\lambda}{\lambda'^4} \quad \text{(II-17)}$$

where $f(\lambda')$ is the filter transmission function and $\Delta\lambda$ the thickness of the spectral segment. The summation is over incident wavelength and extends over an appropriate wavelength range 2δ centered about line center λ.

Output

The code was written to perform the calculations with appropriate tests to limit the number of transitions considered. At high temperatures, several hundred transitions are included. Inputs to the program are the interference filter profiles, dye laser line center and bandwidth, and temperature range of interest. The outputs include the total relative intensities of the anti-Stokes, Stokes, and fundamental Stokes Q branch, the latter with no narrow band filtering. Since absolute intensity estimates can be made of the latter as seen previously, absolute intensity estimates can then be made for the total anti-Stokes and Stokes signals, e.g.,

$$Q_S = \frac{\tilde{Q}_S}{\tilde{Q}_Q} Q_Q \epsilon_S' \quad \text{(II-18)}$$

where tildes indicate relative intensities, and Q_Q is the calculated absolute Stokes Q branch intensity without including the collection efficiency. ϵ_S' is the collection efficiency of the Stokes detector excluding the narrowband interference filter which is already accounted for in Equation (II-15). Separate efficiencies are necessitated by the fact that ϵ_S' and ϵ_A' are not equal because of the spectral characteristics of the various optical elements in the spectrometer, e.g., dichroics, mirrors, etc.

Appendix II - References

II-1 G. Herzberg, Molecular Spectra and Molecular Structure I. Spectra of Diatomic Molecules, D. Van Nostrand Co., Princeton, NJ, 1950.

II-2 E. B. Wilson, J. C. Decius, and P. C. Cross, Molecular Vibrations, McGraw-Hill NY, 1955.

II-3 S. Bhagavantam, Scattering of Light and the Raman Effect, Chemical Publishing Co., Brooklyn, NY, 1942.

Unclassified

SECURITY CLASSIFICATION OF THIS PAGE (When Data Entered)

REPORT DOCUMENTATION PAGE		READ INSTRUCTIONS BEFORE COMPLETING FORM
1. REPORT NUMBER R76-952296-2	2. GOVT ACCESSION NO.	3. RECIPIENT'S CATALOG NUMBER
4. TITLE (and Subtitle) Investigation to Extend the Applicability of Laser Raman Scattering Diagnostics to Practical Combustion Systems		5. TYPE OF REPORT & PERIOD COVERED Technical Report 28 Jan 1976 to 31 Aug 1976 6. PERFORMING ORG. REPORT NUMBER R76-952296-2
7. AUTHOR(s) Alan C. Eckbreth		8. CONTRACT OR GRANT NUMBER(s) ~~8960~~-20 N00014-75-C-1143
9. PERFORMING ORGANIZATION NAME AND ADDRESS United Technologies Research Center East Hartford, CT 06108		10. PROGRAM ELEMENT, PROJECT, TASK AREA & WORK UNIT NUMBERS
11. CONTROLLING OFFICE NAME AND ADDRESS Project SQUID Purdue University West Lafayette, IN 47907		12. REPORT DATE September 30, 1976 13. NUMBER OF PAGES
14. MONITORING AGENCY NAME & ADDRESS (if different from Controlling Office)		15. SECURITY CLASS (of this report) Unclassified 15a. DECLASSIFICATION DOWNGRADING SCHEDULE

16. DISTRIBUTION STATEMENT (of this Report)

Unlimited

DISTRIBUTION STATEMENT A
Approved for public release;
Distribution Unlimited

17. DISTRIBUTION STATEMENT (of the abstract entered in Block 20, if different from Report)

18. SUPPLEMENTARY NOTES

19. KEY WORDS (Continue on reverse side if necessary and identify by block number)

Laser Raman Scattering Diagnostics, Remote Combustion Diagnostics, Laser Modulated Particulate Incandescence, Laser-Particulate Interaction, Raman Amplitude Modulation

20. ABSTRACT (Continue on reverse side if necessary and identify by block number)

Laser Raman scattering techniques for combustion diagnosis have undergone considerable development in the past several years and are now being employed in a number of fundamental flame investigations. However, from an instrumentation viewpoint, practical combustion environments can differ greatly from the flames typically employed in fundamental studies. In particular, pulsed laser Raman thermometry experiments have shown laser modulated particulate (soot) → next page

DD FORM 1 JAN 73 1473 EDITION OF 1 NOV 65 IS OBSOLETE

Unclassified

SECURITY CLASSIFICATION OF THIS PAGE (When Data Entered)

20.

incandescence to be an especially severe problem. Particles in the measurement volume, which, at flame temperatures, are already incandescent and contribute significantly to the total luminous emission, absorb the incident Raman inducing laser radiation, heat to temperatures far above ambient, and emit greatly increased amounts of gray/blackbody radiation which can exceed the sought-for Raman signal levels by several orders of magnitude. Under Project SQUID sponsorship, a detailed study of this phenomenon has been conducted, the results of which are reported herein. Laser irradiated particulate temperatures were determined in a laminar propane diffusion flame as a function of focal flux level and found to agree fairly well with a simple analytical model. In addition to incandescence, laser induced C_2 Swan emissions were also found to be present. The laser induced particulate incandescent noise was found to saturate with increasing laser energy and to decrease in magnitude with shorter focussing lens focal length. Extrapolated improvements in signal to noise ratio with increasing flux levels from $2(10^5)$ to 10^9 W/cm^2 were on the order of a few hundred. The effect of signal averaging Raman data obtained from harsh (luminous, sooty) fluctuating media was analyzed. Ensemble averaging pulsed Raman data leads to quantities dependent not only on average temperature but also on the magnitude and correlations of fluctuations in density and temperature, which can affect measurement accuracy. Temperature measurements were made on a clean flame and a temperature measurement demonstration was performed on a soot seeded laboratory burner using a noise sampling and subtraction approach.

END-17